Electronic Supplementary Material (ESI) for Journal of Materials Chemistry A.

Supporting Information

Organic photoelectrodes engineering: accelerating photocurrent generation *via* donor-acceptor interactions and surface-assisted synthetic approach

Yaroslav S. Kochergin,[a,b] Seyyed Mohsen Beladi-Mousavi,[a] Bahareh Khezri,[a] Pengbo Lyu,[c] Michael J. Bojdys,[d] and Martin Pumera*,[a]

[a] *Department of Inorganic Chemistry, Faculty of Chemical Technology, University of Chemistry and Technology Prague, Technická 5, 166 28 Prague, Czech Republic.*

[b] *Institute of Organic Chemistry and Biochemistry of the CAS, Flemingovo nám. 2, 166 10 Prague, Czech Republic Address here.*

[c] *Institute Charles Gerhardt Montpellier, University of Montpellier, CNRS, ENSCM, Montpellier 34095, France*

[d] *Department of Chemistry, King's College London, Britannia House Guy's Campus, 7 Trinity Street, SE1 1DB, London, UK.*

Table of Contents

Materials.

All air- and moisture-sensitive reactions were carried out under an argon atmosphere using the standard Schlenk technique. All reagents and solvents were used as received without any additional purification steps. 1,3,5-Trihydroxybenzene and 2-mercaptoethanol were purchased from Acros Organics. 5-Bromothiophene-2-carbonitrile and trifluoromethanesulfonic acid (TFMSA) were purchased from ABCR. Tetrakis(triphenylphosphine)palladium(0) was purchased from Sigma-Aldrich. Completion of reactions was determined by TLC using silica gel (Merck 60, F-254) covered aluminium plates and visualized by UV irradiation. Column chromatography purification was performed using silica gel (0.063–0.2 mm, 100 mesh, ASTM) from Acros Organics.

Structural Characterisation.

NMR spectra of the monomers were recorded on Bruker Advance 400 MHz spectrometer with $CDCl_3$ as the internal standard, which was set at $\delta_H = 7.26$ ppm. **NMR spectra of the polymers in solid state** were measured *via* ^{13}C cross-polarization magic-angle-spinning (CP-MAS) with MAS rate of 12.0 kHz using 4 mm diameter zirconia rotors. Contact time was 10 ms and a relaxation delay - 10.0 s.

Crystal structure of polymers was characterized *via* **powder X-ray diffraction (PXRD**) using Bruker AXS D8 Advanced SWAX diffractometer with Cu Kα ($\lambda = 0.15406$ nm) as a radiation source.

Fourier transform infrared (FTIR) spectra of the materials were recorded with the attenuated total reflection (ATR) technique on an AVATAR 370 FT-IR spectrometer from Thermo Nicolet.

Elemental analyses (C, H and N) were performed using a PE 2400 Series II CHN Analyzer.

Inductively coupled plasma optical emission spectrometry (ICP-OES) measurements were performed using the SPECTRO ARCOS optical emission spectrometer (SPECTRO Analytical Instruments, Kleve, Germany) with radial plasma observation.

Scanning electron microscopy (SEM) imaging was done on a Tescan Maia3 microscope equipped with an energy-dispersive X-ray (EDS, Oxford Instruments) detector.

Transmission Electron Microscope (TEM) images and selected area electron diffraction (SAED) were carried out using a JEM-1011instrument (JEOL), operating at an accelerating voltage of 80 kV with a spherical aberration coefficient value of 5.6 mm. Images were recorded on VELETA - side-mounted TEM CCD (charge-coupled device) camera with a resolution of 2K x 2K and with an exposure time of one second per frame and an interval of two seconds between the frames.

Fourier transform infrared (FTIR) spectra were recorded with attenuated total reflection (ATR) technique on an AVATAR 370 FT-IR spectrometer from Thermo Nicolet. NICOLET iS50R FTIR spectrometer (Thermo Scientific). A Diamond ATR crystal and a DTGS detector was used for the measurement in the range of 4000–400 cm^{-1} at a resolution of 4 cm^{-1}.

X-ray photoelectron spectroscopy (XPS) was performed using a SPECS spectrometer equipped with an XR 50 MF monochromatic X–ray radiation source (1486.7 eV) and a Phoibos 150 2D CCD hemispherical analyser and detector. The pressure inside the chamber during the measurements was $5x10^{-10}$ mbar or lower. Wide-scan surveys were performed with Ep=80 eV, with subsequent high-resolution scans of the desired core lines with Ep=60 eV. The samples were placed on double-sided carbon tape. The binding energy values are referenced to the adventitious carbon peak at 284.8 eV.

Thermogravimetry analysis (TGA) was performed on Setsys Evolution 18 thermal analyser from Setaram under air and nitrogen atmosphere with the heating rate of 10 ^oC/min and maximum temperature of 1000 ^oC.

Solid State UV/Vis measurements were carried out on Cary 6000i UV-Vis-NIR spectrometer from Agilent in reflection mode. The samples were prepared by spreading the polymer powder as a thin film between two quartz microscopic slides.

Solid state fluorescence spectra were recorded using a Fluorolog Extreme (Horiba) system equipped with a Xe lamp (450 W) and a double excitation monochromator. An iHR320 monochromator with a thermoelectrically cooled PMT detector was used for the measurement of emission spectra.

Gas Sorption Analyses. N_2 adsorption/desorption measurements were performed on the Quantachrome Instruments Autosorb 1C surface area analyser at 77 K. Samples were degassed at 120 C for 15 h under vacuum (10^{-5} Bar) before analysis. Brunauer-Emmett-Teller (BET) surface area (S_{BET}) was calculated in the relative pressure range (p/p_0) from 0.05 to 0.35. Pore size distribution was calculated using Barrett-Joyner-Halenda (BJH) pore model. The H_2 adsorption (at 77 K) and CO_2 adsorption/desorption (at 298 K) isotherms were recorded using an ASAP 2020 (Micromeritics, USA) volumetric instrument.

Contact angle measurements. Wettability study was performed using See System E instrument (Advix Instruments). For the measurement, 5 µL water drop was deposited on to a silica substrate covered with the polymeric material. The measurement was repeated 5 times for each material and the average angle was derived.

PEC Measurements. For PEC measurements, prepared polymers were deposited on a commercial ITO glass by means of spray-coating. For this purpose, the polymer was dispersed in acetone (1 mg mL^{-1}) and sonicated for 15 minutes. The coated area was calculated to be 0.36 cm^2 and was kept similar for all measurements, the uncovered part of ITO glass was protected with a Teflon tape. The fabricated photoanodes were used as working electrodes in a three-electrode setup with a counter electrode (Pt wire), and a reference electrode (Ag/AgCl). The simulated sunlight was from a 300 W short-arc Xenon lamp (100 mW cm^{-2}, measured with a light intensity meter from Torr Labs) with a UV blocking coating to prevent ozone generation

(Newport). The electrolyte for PEC measurements - 0.01 M Na_2SO_4, was degassed with argon for 30 min prior to measurements. Galvanostat / potentiostat (Autolab PGSTAT 302V, Metroohm) was used to measure the LSV characteristic of the electrodes, with 1 mV s^{-1} scan rate, and there is no correction on data for any losses of the uncompensated resistance. Current density was calculated from the photoelectrode area (0.36 cm^2) exposed to the light source divided by the photocurrent value achieved at 0.6 V bias *vs*. Ag/AgCl. The EIS spectra were recorded by applying a 10 mV AC signal in the frequency range from 100 000 to 0.01 Hz at applied potential of 0.6 V *vs*. Ag/AgCl. Chronoamperometry measurements were conducted at a constant potential of 0.6 V *vs*. Ag/AgCl. Photoelectrocatalytic OER experiments were conducted using 1 M NaOH as an electrolyte.

Materials Synthesis.

On-copper polymerization protocol. For the polymerization reaction, a commercial-grade copper plate (20 x 20 cm and 0.1 cm thickness) was cut into equal parts to ensure that they will fit into the reaction vessel. Before usage, the copper plates were washed under ultrasound in 1 M HCl, acetone, and ethanol for 15 min each. Subsequently, the plates were dried under vacuum. The respective triethynyl-substituted monomer was dissolved in 10 mL of pyridine and added dropwise to a 100 mL reaction vessel charged with copper plates submerged in 40 mL of pyridine. The mixture was kept under ambient atmosphere without stirring at 60 °C for 48 h. The residual monomers and oligomers were washed from the copper support with hot DMF and acetone, and the polymer on copper was dried under reduced pressure. To detach the polymer films from the copper substrate, the later was treated with an aqueous solution of ammonium persulfate (0.5 M). Within seconds, polymer films were released from the copper substrate (**Figure S1**). The as-synthesized films were subjected to a wash with hot DMF, THF, MeOH, water, and acetone and dried in a vacuum oven at 120°C overnight.

Bulk polymerization protocol. The reaction flask was charged with the respective triethynyl-substituted monomer and copper (I) chloride, and subsequently pyridine was added to the reaction mixture. The reaction was then kept stirring at 60 °C under ambient atmosphere for 3 days. The formed precipitate was collected by filtration and washed with hot DMF, THF, MeOH, water ,and acetone. Further, the obtained powder was subjected to Soxhlet extraction using THF and MeOH as washing solvents. In the end, the product was dried in a vacuum oven at 120 °C overnight.

Synthetic Protocols and Schemes

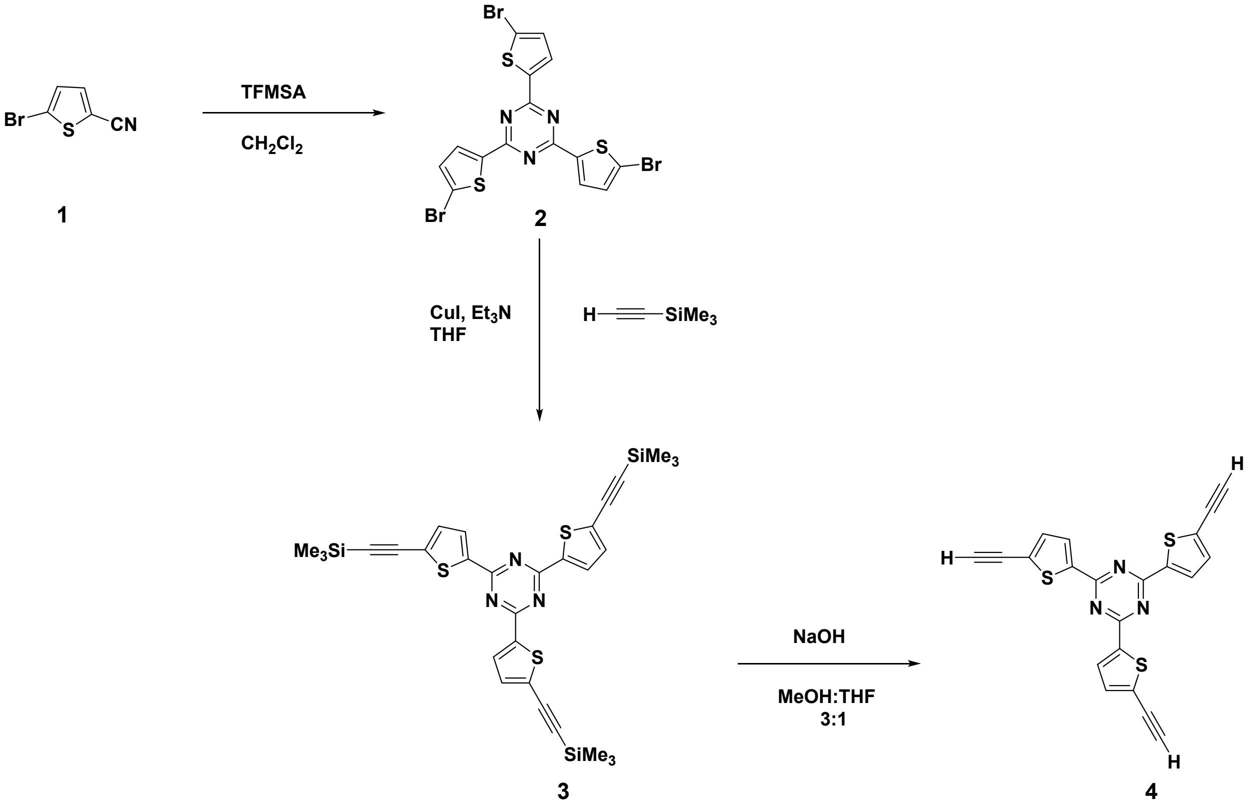

Scheme S1. Total synthesis of 2,4,6-tris(5-ethynylthiophen-2-yl)-1,3,5-triazine (**4**).

*2,4,6-Tris(5-bromothiophene-2-yl)-1,3,5-triazine **(2)*** was prepared according to reported protocol by Yasuda *et al.*[1]
Stirred solution of 5-bromothiophene-2-carbonitrile (**1**) (3.0 g, 16 mmol) in dry CH_2Cl_2 (40 mL) was cooled down to 0 °C, subsequently, trifluoromethanesulfonic acid (3.6 g, 24 mmol) was added dropwise. The mixture was stirred at room temperature for 36 h. After removal of the solvent under reduced pressure, the residue was neutralized with an aqueous $NaHCO_3$. The formed precipitate was collected by filtration and washed with water, methanol, acetone, and hexane in this order, and then dried under vacuum to afford desired product as an off-white solid (2.6 g, 29% yield). ^{1}H NMR (400 MHz, $CDCl_3$, δ/ppm): 7.99 (t, *J* = 4.0 Hz, 3H), 7.19 (d, *J* = 4.0 Hz, 3H).

2,4,6-tris(5-((trimethylsilyl)ethynyl)thiophen-2-yl)-1,3,5-triazine (**3**) and *2,4,6-tris(5-ethynylthiophen-2-yl)-1,3,5-triazine* (**4**) were synthesized according to protocol by Maragani *et al.*[2]

2,4,6-Tris-(4-ferrocenylethynyl-phenyl)-1,3,5-triazine (**3**)
Starting s-triazine **2** (1 g, 1.78 mmol) was suspended in THF (80 mL), and triethylamine (5 mL). Subsequently, $Pd(PPh_3)_4$ (0.072 g, 0.06 mmol), trimethylsilylacetylene (0.70 g, 7.14 mmol) and copper(I) iodide (0.017 g, 0.03 mmol) were added under argon atmosphere, and the reaction mixture was stirred at 60 ^{o}C for 16 h. After completion of the reaction, the reaction mixture was filtered through a Celite pad and concentrated under reduced pressure. The crude compound was purified by column chromatography on silica gel using hexane : $CHCl_3$ 5:1 as eluent to get the desired product **3** as a yellow oil (0.88 g, 80%); ^{1}H NMR (400 MHz, $CDCl_3$, δ/ppm): δ = 8.08 (d, *J* = 3.9 Hz, 3H), 7.29 (d, 3H, *J* = 3.9 Hz, 3H), 0.3 (s, 27H) ppm; ^{13}C NMR (100 MHz, $CDCl_3$): δ = 166.90, 141.75, 133.58, 131.37, 129.81, 102.43, 97.29, 0.25 ppm.

2,4,6-Tris-(4-ferrocenylethynyl-phenyl)-1,3,5-triazine (**4**)
The TMS-protected s-triazine **3** (0.86 g, 1.4 mmol) was dissolved in the mixture (3:1 v/v) of methanol (90 mL) and THF (30 mL). 3N aqueous solution of NaOH (20 mL) was added and the reaction mixture was stirred at room temperature for 1 h. After completion of the reaction, the product was extracted with DCM, washed with brine and dried over anhydrous $MgSO_4$. Solvents were removed under reduced pressure to give target compound **4** as a yellow solid (0.36 g, 65%); ^{1}H NMR (400 MHz, $CDCl_3$, δ/ppm): δ = 8.12 (d, *J* = 3.9 Hz, 3H), 7.36 (d, *J* = 3.8 Hz, 3H), 3.54 (s, 3H); ^{13}C NMR (100 MHz, $CDCl_3$): δ = 166.96, 142.02, 134.17, 131.44, 128.62, 84.08.

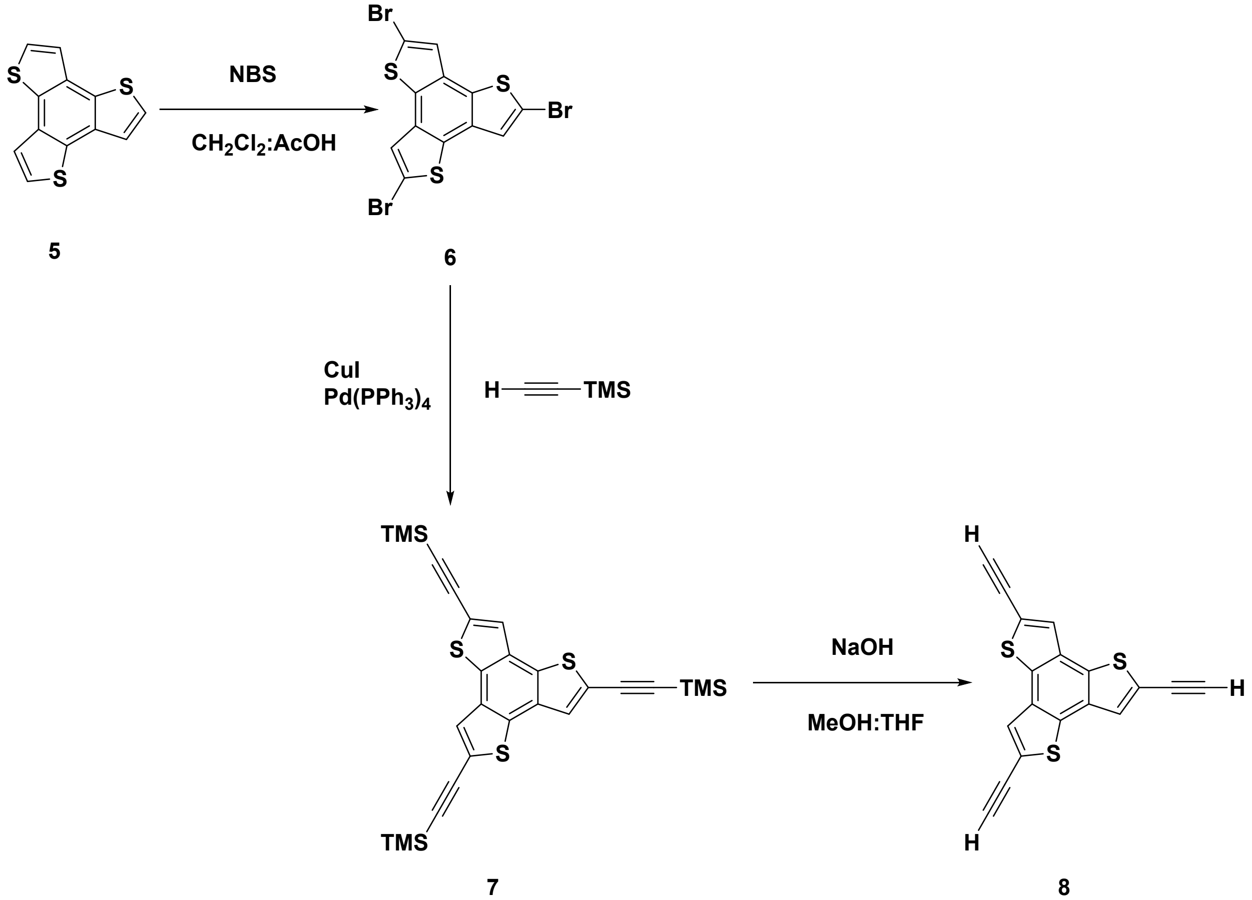

Scheme S2. Total synthesis of 2,5,8-Triethynylbenzo[1,2-b:3,4-b':5,6-b'']trithiophene. (**8**).

Benzo-[1,2-b:4,5-b′:5,6-b′′]trithiophene (**5**) was prepared according to previously published protocol.[3]
2,5,8-Tribromobenzo[1,2-b:3,4-b′:5,6-b′′]trithiophene (**6**) was synthesized following the protocol from Kashiki *et al.*[4]

2,5,8-Tribromobenzo[1,2-b:3,4-b':5,6-b'']trithiophene (**6**)

To a well-stirred solution of **5** (0.31 g, 1.27 mmol) in mixture (4:1 v/v) of DCM (10 mL) and acetic acid (2.5 mL) under nitrogen atmosphere was portion wise added N-bromosuccinimide (0.68 g, 3.84 mmol). The reaction mixture was stirred at room temperature for 60 h, and then quenched with water (20 mL). The formed precipitate was collected by filtration, washed with water (2x10 mL) and ethanol (2x10 mL), and dried under reduced pressure. Recrystallization from chlorobenzene gave desired compound **6** as pale violet solid (0.12 g, 22%). ^{1}H NMR (400 MHz, $CDCl_3$, δ/ppm): δ = 7.52 (s, 3H). Anal. Calcd for $C_{12}H_3S_3Br_3$: C, 29.84; H, 0.63%. Found: C, 30.69; H, 0.75%.

2,5,8-Tri(trimethylsilylethynyl)benzo[1,2-b:3,4-b':5,6-b'']trithiophene (**7**) and *2,5,8-Triethynylbenzo[1,2-b:3,4-b':5,6-b'']trithiophene* (**8**) were prepared according to manuscript by Hong *et al.*[5]

2,5,8-Tri(trimethylsilylethynyl)benzo[1,2-b:3,4-b':5,6-b'']trithiophene (**7**)

2,5,8-tribromobenzo[1,2-b:3,4-b':5,6-b'']trithiophene **6** (0.70 g, 1.45 mmol), copper(I) iodide (0.082 g, 0.43 mmol) and $Pd(PPh_3)_4$ (103 mg, 0.09 mmol) were suspended in the mixture (4:1 v/v) of Et_3N (30 mL) and THF (120 mL). Subsequently, trimethylsilylacetylene (1.4 mL, 9.86 mmol) was added. The reaction mixture was stirred under nitrogen and heated to reflux overnight. After completion of the reaction, the mixture was filtered through a Celite pad and evaporated to dryness under reduced pressure. The crude product was purified by column chromatography on silica gel using hexane as eluent. Subsequent recrystallization by layering methanol onto a concentrated DCM solution yielded the desired product **7** as a white solid. Yield: 0.32 g (42 %). ^{1}H NMR (400 MHz, $CDCl_3$, δ/ppm): δ = 7.68 (s, 3H), 0.33 (s, 27H) ppm; ^{13}C NMR (100 MHz, $CDCl_3$): δ = 132.89, 130.33, 127.31, 122.80, 101.85, 97.10, 0.21 ppm.

2,5,8-Triethynylbenzo[1,2-b:3,4-b':5,6-b'']trithiophene (**8**)

To a stirred solution of 2,5,8-tri(trimethylsilylethynyl)benzo[1,2-b:3,4-b':5,6-b'']trithiophene **7** (0.26 g, 0.49 mmol) in mixture (1:1 v/v) of THF (35 mL) and MeOH (35 mL) was added K_2CO_3 (0.42 g, 3.04 mmol). The reaction mixture was stirred at room temperature under nitrogen overnight. The yellow precipitate was filtered and washed with methanol. After drying under vacuum, the target product 8 was isolated as a pale yellow solid (0.13 g, 86 %). ^{1}H NMR (400 MHz, $CDCl_3$, δ/ppm): δ = 7.70 (s, 3H), 3.52 (s, 3H).

Results and Discussion

Surface-Assisted Reaction Workup

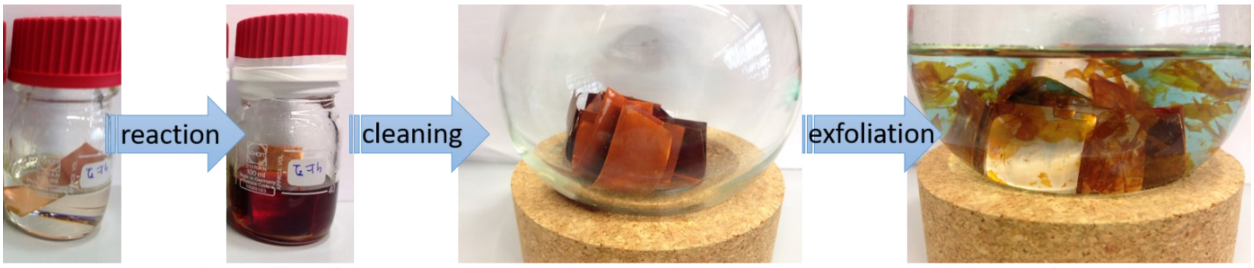

Formation of the polymer film

Hot solvent wash and drying

Release of the polymer film with 0.5 M aqueous $(NH_4)_2S_2O_8$

Figure S1. Photographs of the **Tz-Th@Cu** reaction work-up.

Scanning Electron Spectroscopy

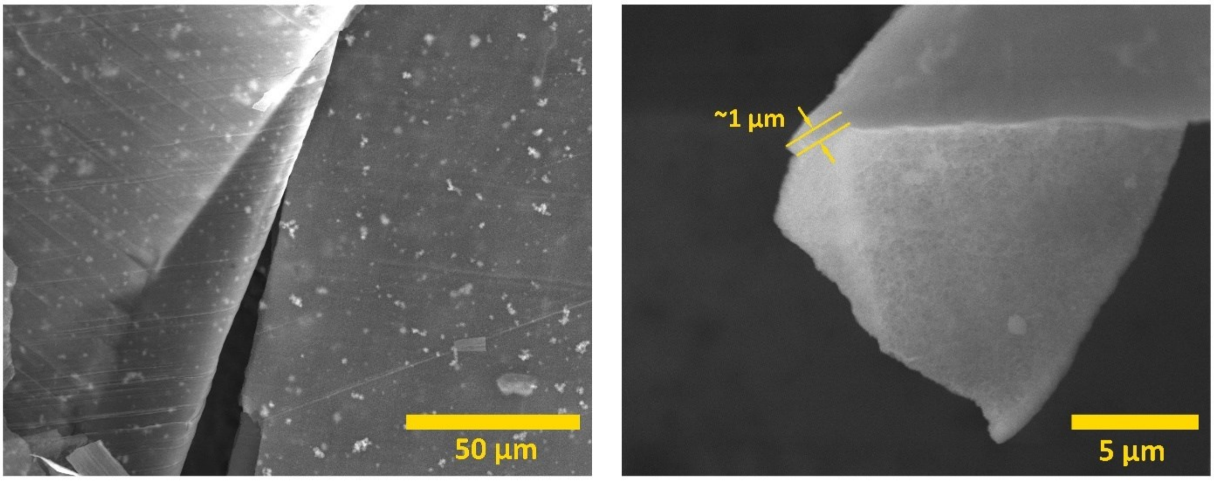

Figure S2. SEM images of **Tz-Th@Cu** polymer.

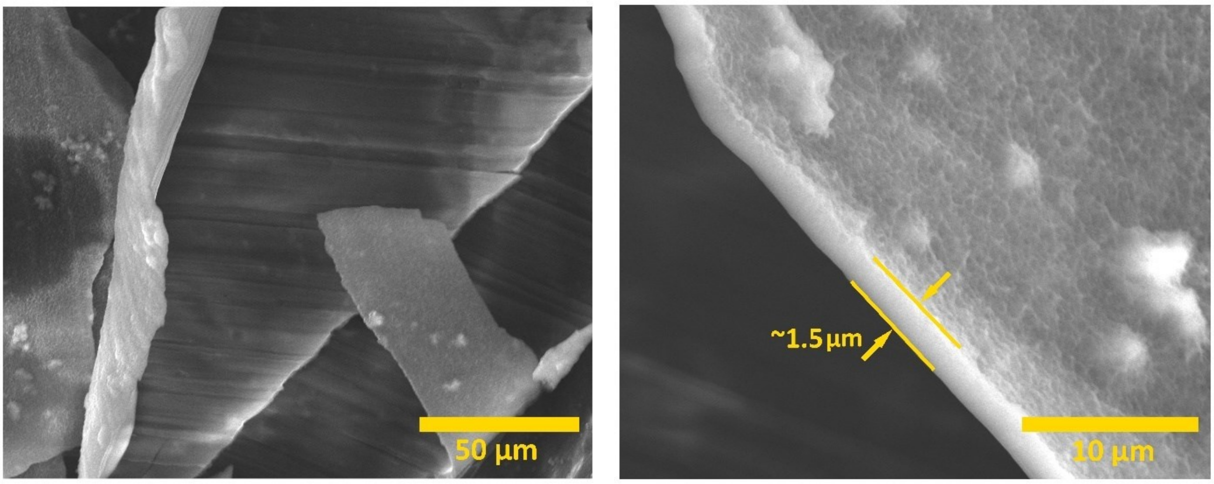

Figure S3. SEM images of **BTT@Cu** polymer.

Atomic Force Microscopy

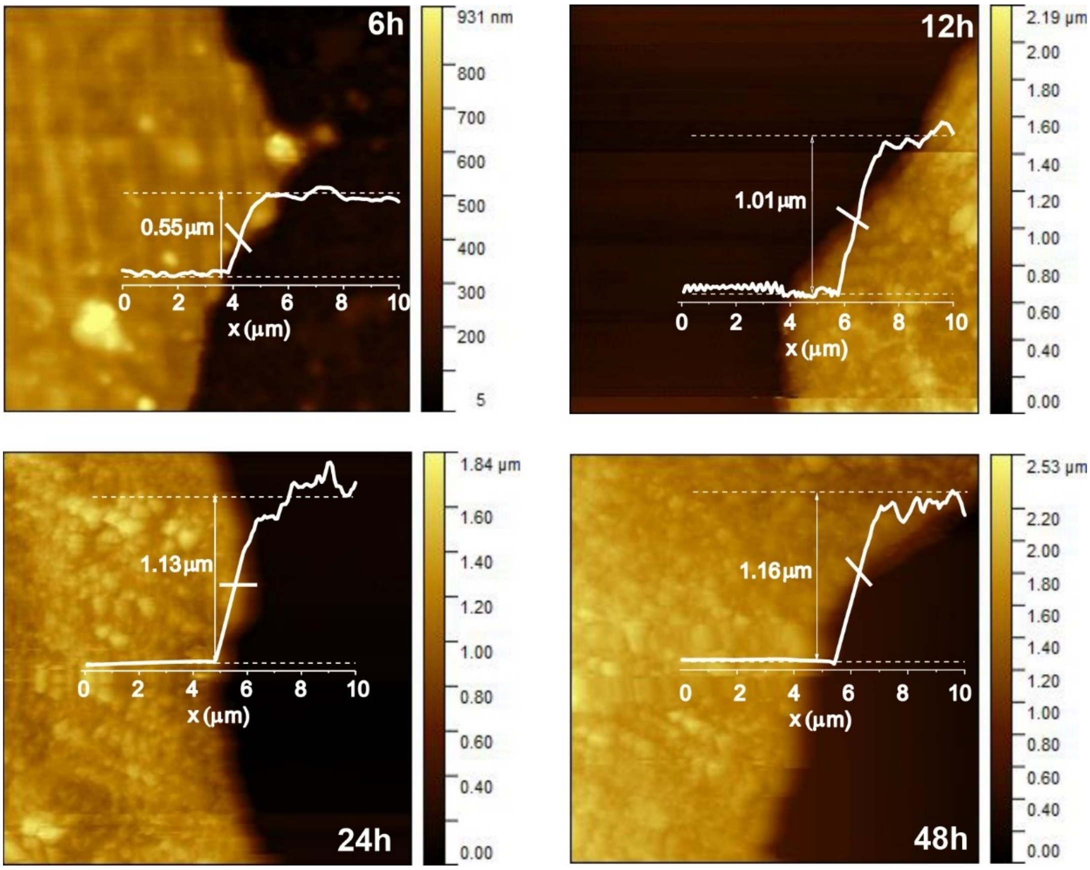

Figure S4. AFM images of Tz-Th@Cu flakes after designated reaction time. In the insets – cross-section profiles

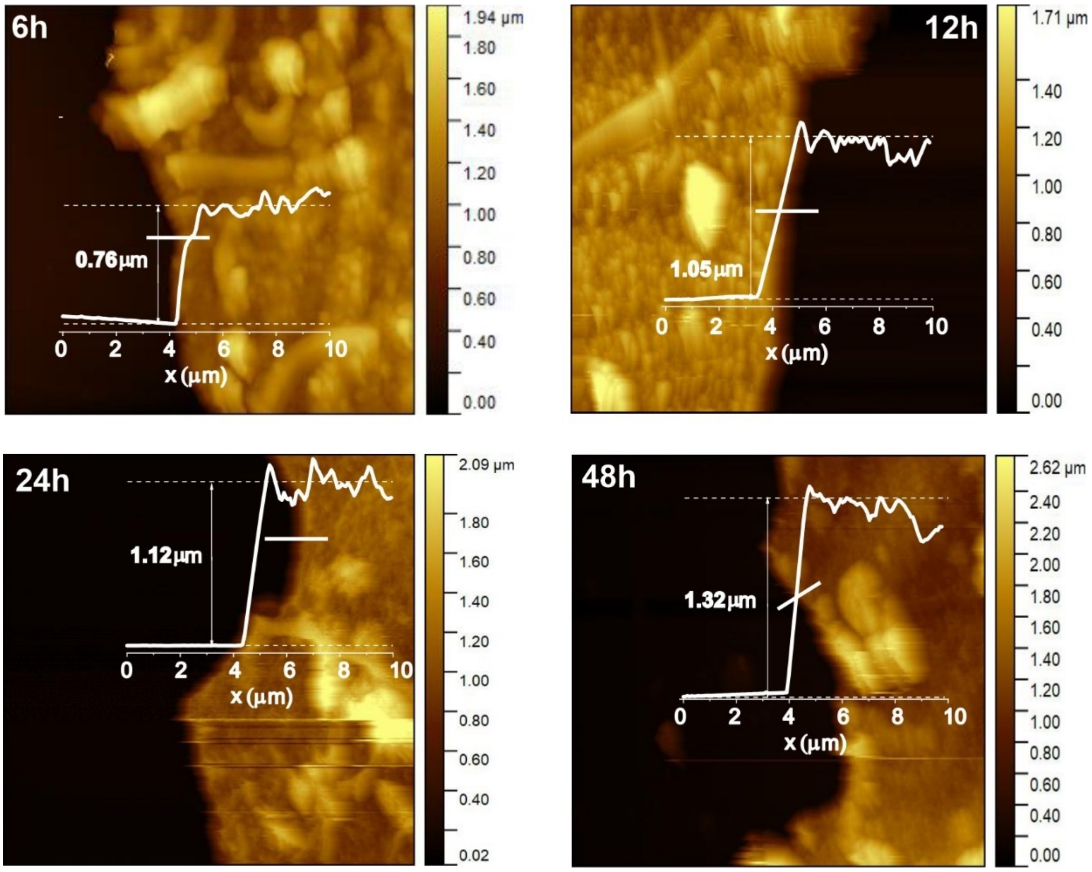

Figure S5. AFM images of Tz-Th@Cu flakes after designated reaction time. In the insets – cross-section profiles

Elemental Analyses

Table S1. EA and ICP-OES data (in wt%) for **Tz-Th@Cu**

Elemental composition	C	H	N	S	C/N	C/S	Cu	P
Calculated	**63.62**	**1.53**	**10.60**	**24.26**	**6.00**	**2.62**	1.81	0.38
Found	53.37	2.69	9.42	17.66	5.67	3.02		

Table S2. EA and ICP-OES data (in wt%) for **BTT@Cu**

Elemental composition	C	H	N	S	C/S	Cu	P
Calculated	**68.55**	**0.96**	**-**	**30.49**	**2.25**	n/d*	n/d*
Found	52.40	2.54	1.53	21.04	2.49		

*n/d – not detected

Energy-Dispersive X-ray Spectroscopy

Table S3. EDS data (in wt%) for **Tz-Th@Cu**

Elemental composition	C	H	N	S	C/N	C/S	Cu	O
Calculated	**63.62**	**1.53**	**10.60**	**24.26**	**6.00**	**2.62**	2.49	9.87
Found	56.80	n/a*	16.56	14.14	3.43	4.01		

Table S4. EDS data (in wt%) for **BTT@Cu**

Elemental composition	C	H	N	S	C/S	Cu	O
Calculated	**68.55**	**0.96**	**-**	**30.49**	**2.25**	2.48	8.46
Found	63.44	n/a*	n/d	25.24	2.51		

*n/a – not analysed

Thermogravimetric Analysis

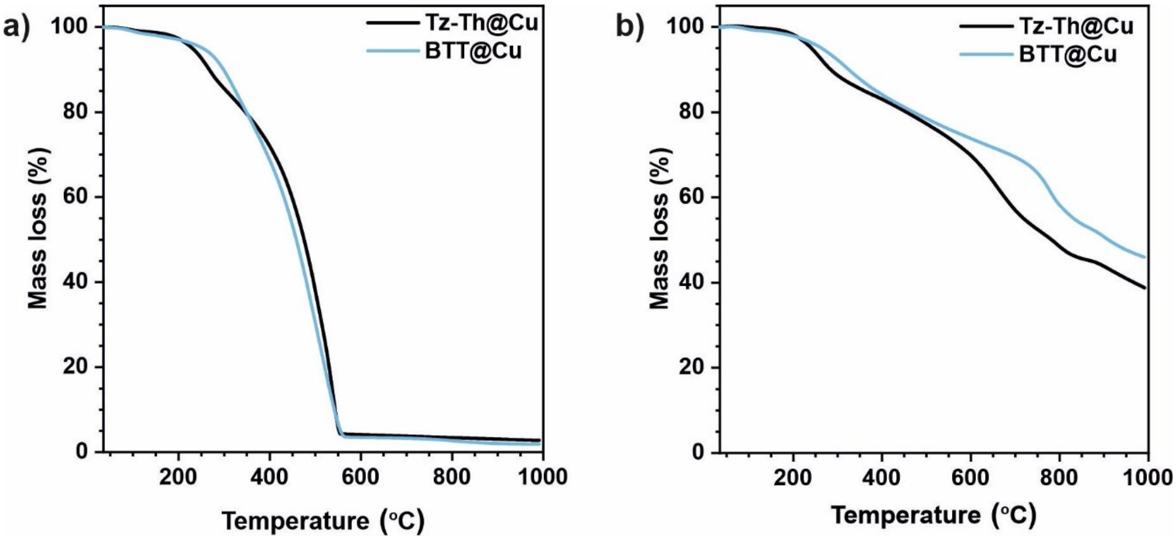

Figure S6. TGA data of **Tz-Th@Cu** (black) and **BTT@Cu** (blue) polymers heated up to 1000 ^{o}C with heating rate of 10 deg. min^{-1} under air **(a)** and heated under N$_2$ **(b)** atmosphere.

X-Ray Photoelectron Spectroscopy

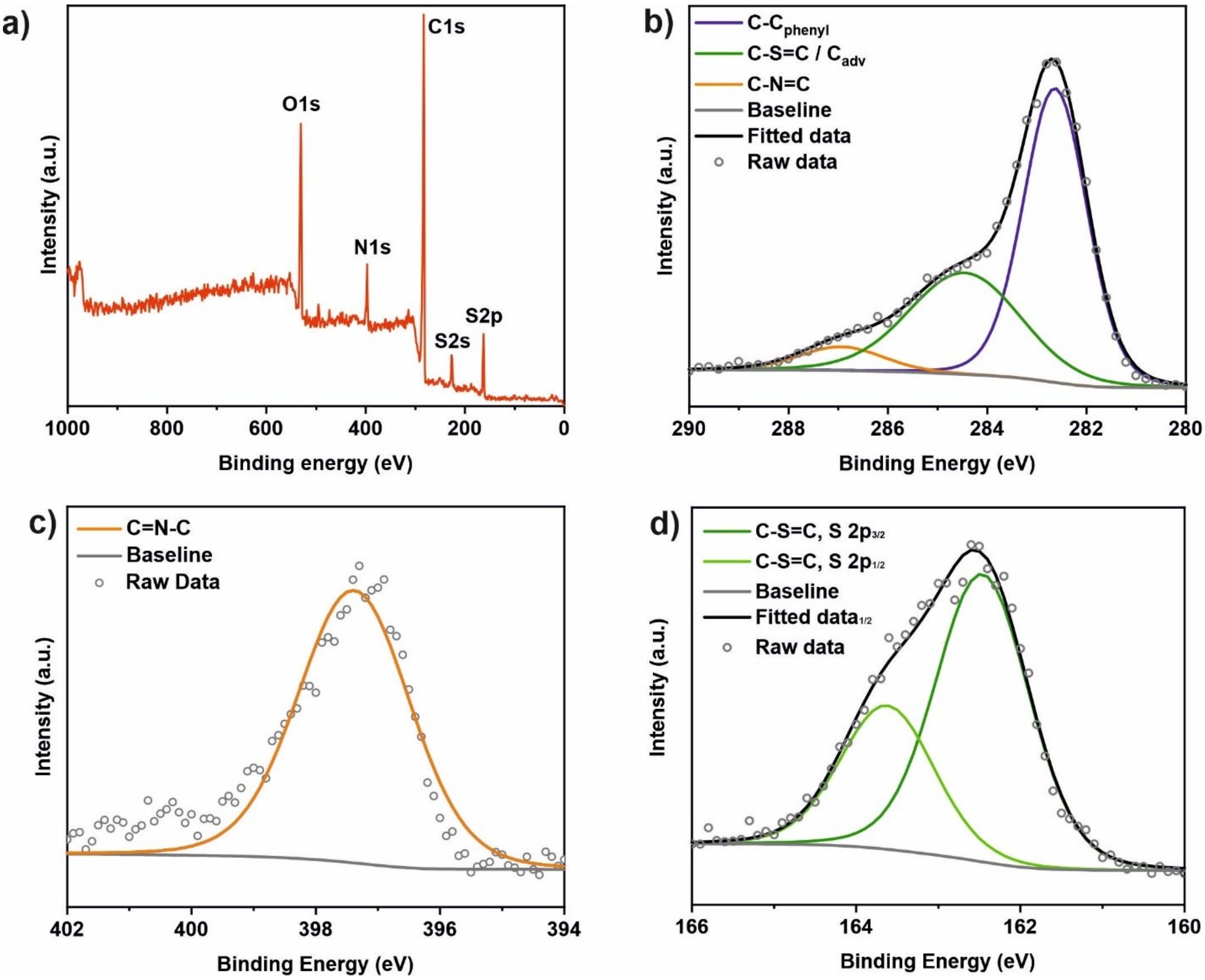

Figure S7. XPS spectra of **Tz-Th@Cu**: (**a**) survey spectra; high resolution deconvoluted spectra of C 1s (**b**), N 1s (**c**), and S 2p (**d**) regions.

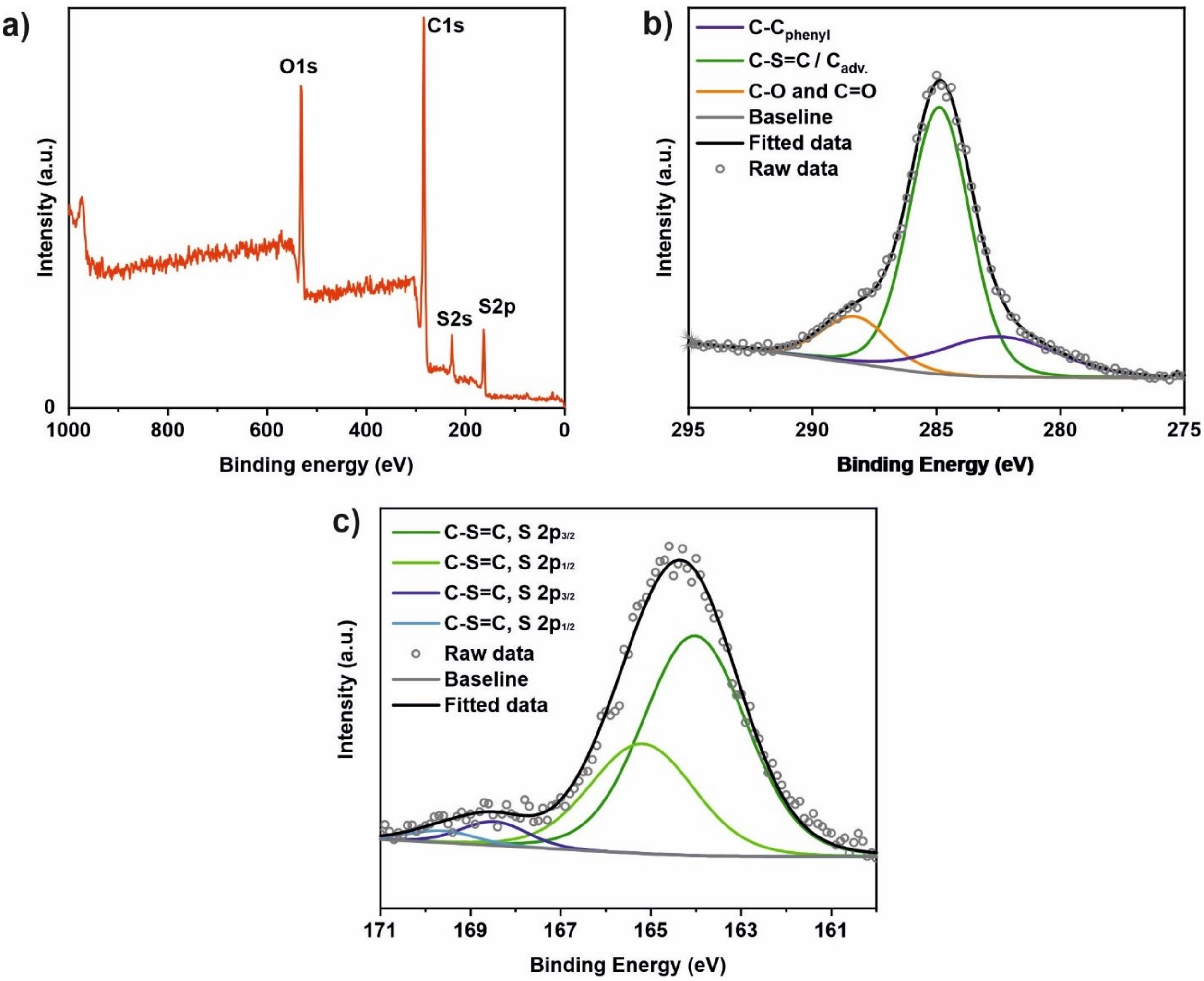

Figure S8. XPS spectra of **BTT@Cu**: (**a**) survey spectra; high resolution deconvoluted spectra of C 1s (**b**) and S 2p (**c**) regions.

Powder X-ray Diffraction Patterns

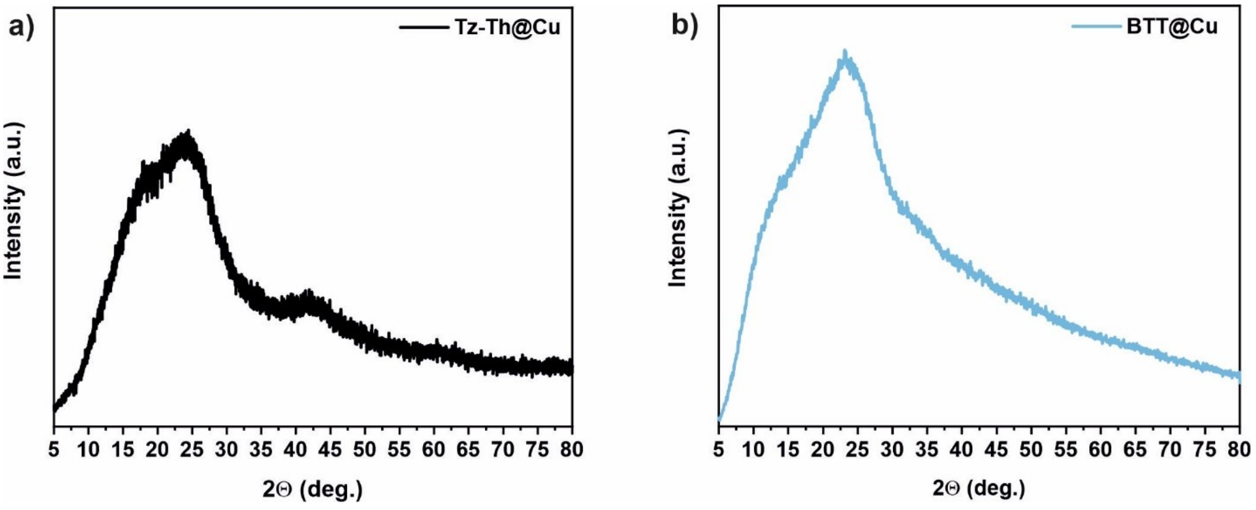

Figure S9. PXRD patterns of **Tz-Th@Cu** (a) and **BTT@Cu** (b) in the range from 0 to 80 deg. 2θ.

Transmission Electron Spectroscopy

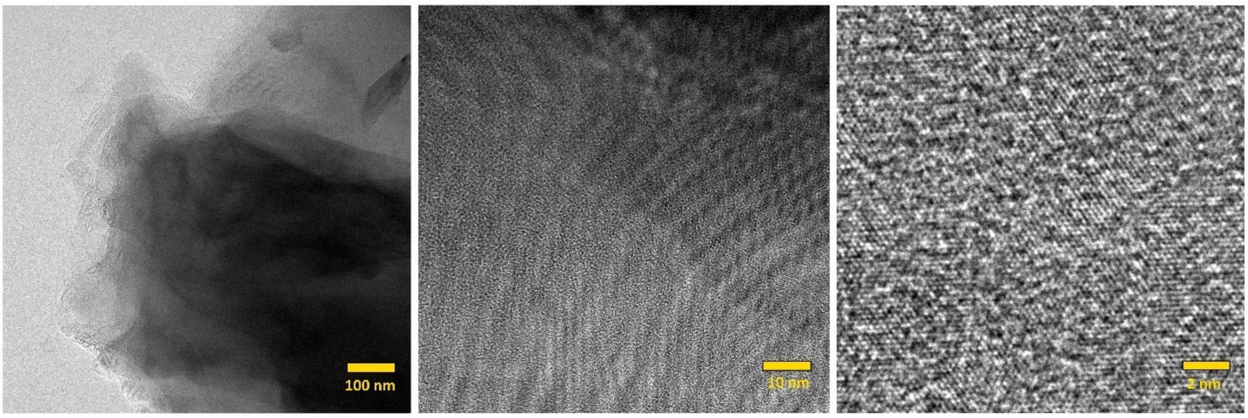

Figure S10. TEM images of **Tz-Th@Cu** at different scales.

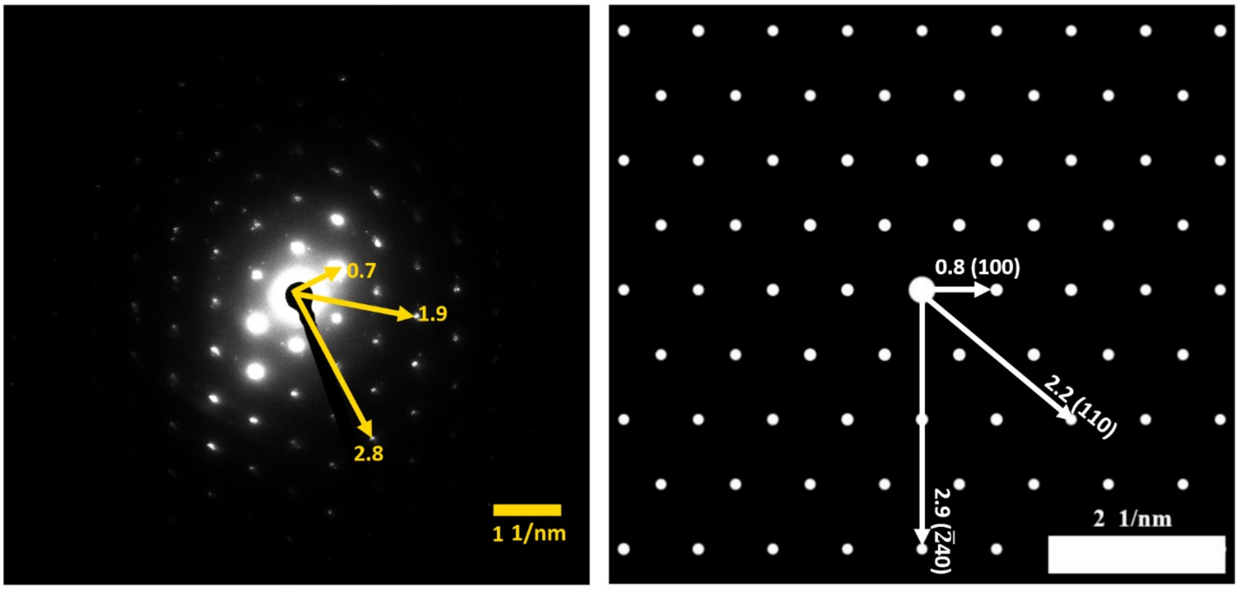

Figure S11. Experimental (left) and simulated for a monolayer (right) SAED patterns of **Tz-Th@Cu** (distances are given in nm^{-1}, corresponding lattice planes are written in parenthesis).

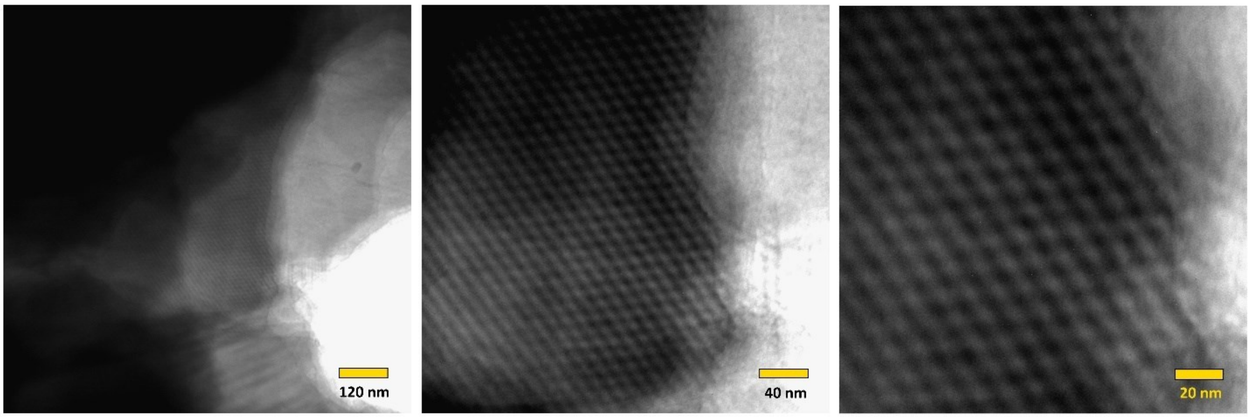

Figure S12. TEM images of **BTT@Cu** at different scales.

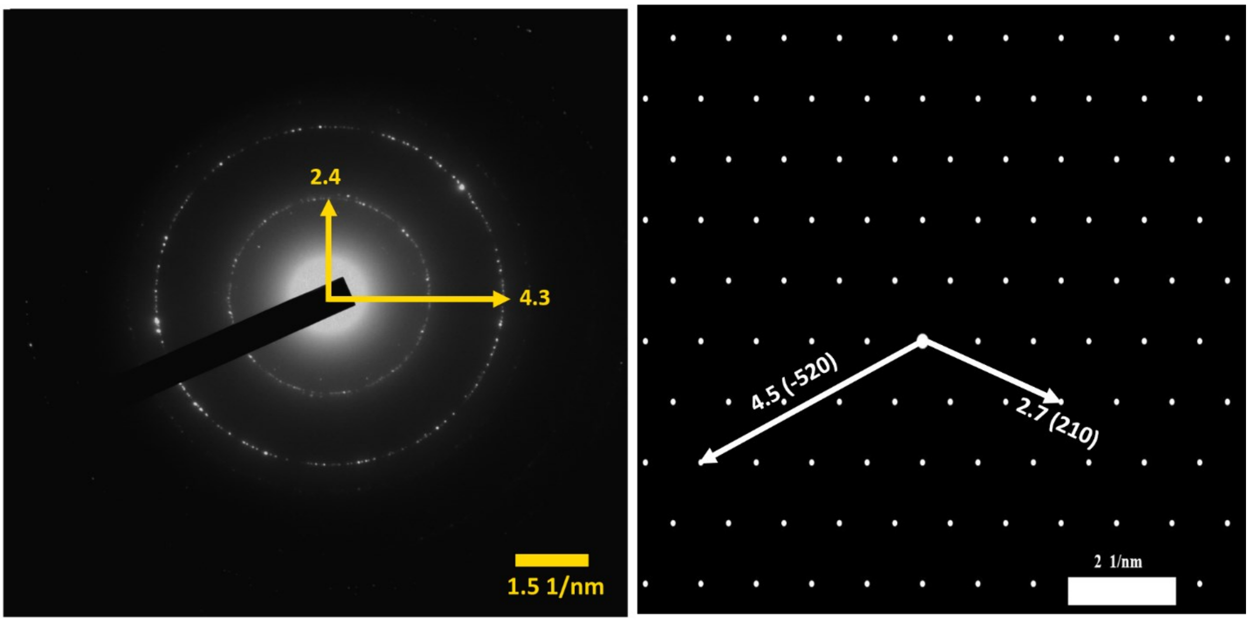

Figure S13. Experimental (left) and simulated for a monolayer (right) SAED patterns of **BTT@Cu** (distances are given in nm^{-1}, corresponding lattice planes are written in parenthesis).

Porosity Analyses

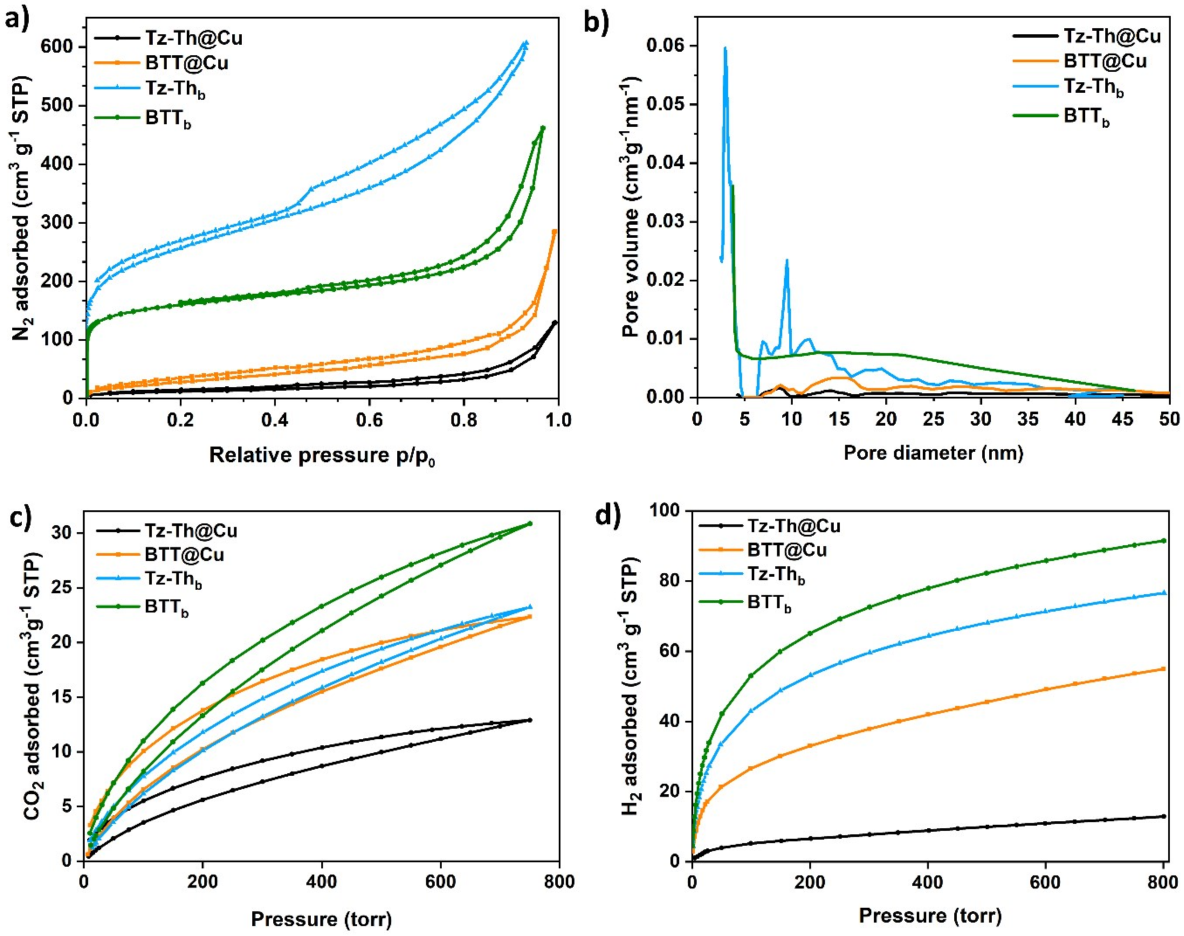

Figure S14. Gas adsorption and porosity analysis preformed for all obtained frameworks: a) N_2 ad-/desorption isotherms measured at 77 K; b) Pore size distribution analysis calculated using Horvath-Kawazoe (HK) method for the region from 0 to 2 nm and Barrett–Joyner–Halenda (BJH) model for the region from 2 to 10 nm; c) CO_2 ad-/desorption isotherms measured at 298 K and 1 bar; d) H_2 adsorption isotherms recorded at 77 K and 1 bar.

Computational Details

The DFT calculations were performed using the projector augmented wave (PAW) [6] formalism within the generalized gradient approximation (GGA) method with Perdew-Burke-Ernzerhof (PBE) exchange-correlation functional as implemented in Vienna Ab Initio Simulation Package (VASP).[7] [8] [9] The cut-off energy of 800 eV for the plane-wave basis set has been consistently used in all calculations. The convergence criterion of 0.01 was used for the forces in geometry optimizations and 10^{-5} eV was used for the energy convergence. The bulk structures were fully relaxed during optimizing. In cases of monolayer, the structure was optimized under constant volume constrain and the vacuum region was set to be larger than 15 Å to avoid the artificial interlayer interactions. Gamma point sampling was used for monolayer and 1×1×2 mesh of *k*-point samplings[10] were used for bulk structure optimizations. The band structures are plotted along the *k* path along the high symmetry points: G (0, 0, 0) →M (1/2, 0, 0) →K (1/3, 1/3, 0) →G (0, 0, 0) for monolayer and G (0, 0, 0) →M (1/2, 0, 0) →K (1/3, 1/3, 0) →H (1/3, 1/3, 1/2) →L (1/2, 0, 1/2) →A(0, 0, 1/2) →G (0, 0, 0) for bulk structures.

Results

1. BTT and Tz-Th monolayers

According to the synthesis scheme, for the polymers produced by [2+2+2] cycloaddition (**Cyclo**), only 1 monolayer is possible for each of **BTT-** (**BTT-Cyclo**) and **Tz-Th-** (**Tz-Th-Cyclo**) based materials, as shown in **Figure S23a** and **S23d**, respectively.

For the polymers produced by Glaser coupling (**Glaser**), there are two different possible monolayers for each of **BTT**- and **Tz-Th-**based materials. The two different monolayers of **BTT-Glaser** are shown in **Figure S23b** (monolayer-1) and **S23c** (monolayer-2), while those of **Tz-Th-Glaser** are shown in **Figure S23e** (monolayer-1) and **S23f** (monolayer-2), respectively. The difference between monolayer-1 and 2 is the orientations of the neighbouring knots.

For **BTT-Glaser**, monolayer-1 and 2 have similar stability; for **Tz-Th-Glaser**, monolayer-1 is more stable by ~ 10 kJ mol^{-1}. Although the monolayers have similar stability (thus possibly co-exist in the bulk structures in a random fashion), for computational convenience, only the monolayer-1 for each polymer (shown in **Figure S23b** and **S23e**, respectively) were chosen for bulk calculations.

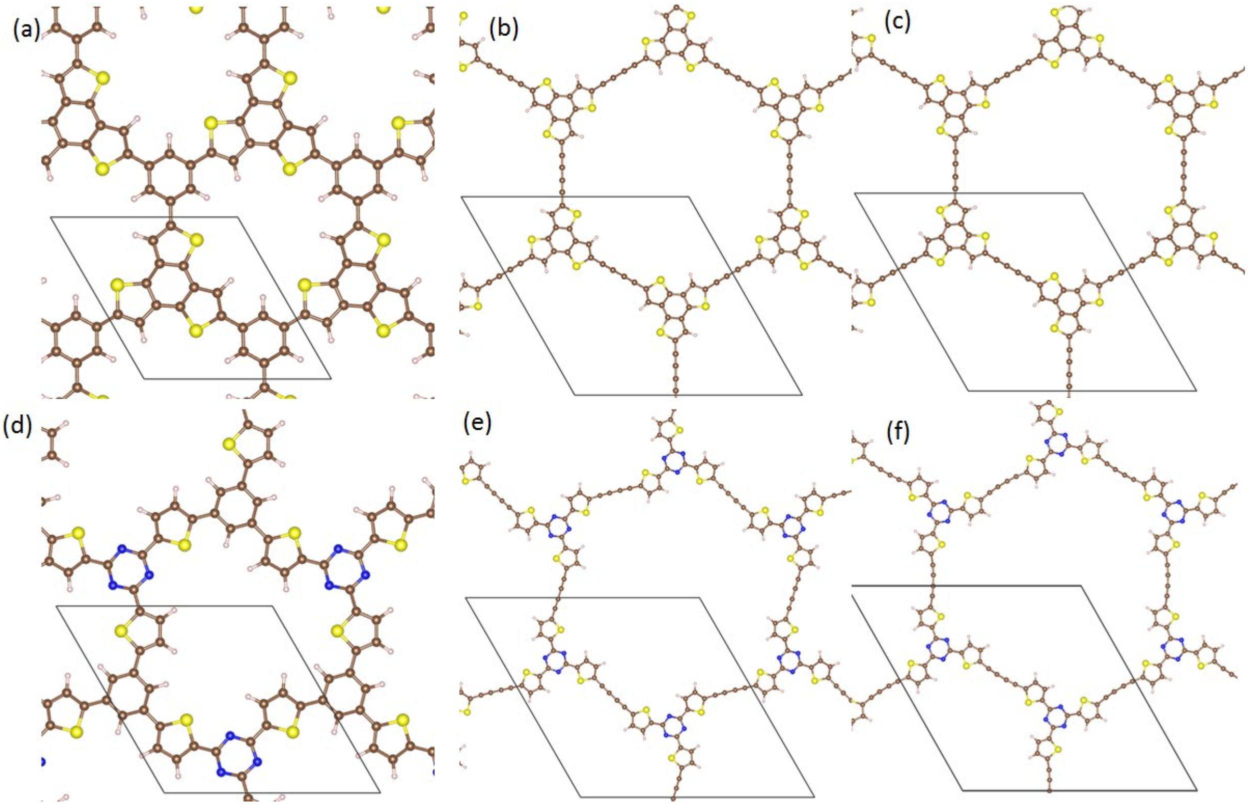

Figure S15. Top views of (a) **BTT-Cyclo** monolayer; (b) **BTT-Glaser** monolayer 1; (c) **BTT-Glaser** monolayer 2; (d) **Tz-Th-Cyclo** monolayer; (e) **Tz-Th-Glaser** monolayer 1 and (f**) Tz-Th-Glaser** monolayer 2. Blue, brown, yellow and white indicate N, C, S and H atoms, respectively.

2. BTT and Tz-Th bulk structures

The interaction energy per unit cell (E_{int}) of bulk structures are defined as:

$E_{\mathrm{int}}=E_{\mathrm{tot}}(\mathrm{bulk}) - E_{\mathrm{tot}}(\mathrm{ML}) \times 2$,

where E_{tot}(bulk) and E_{tot}(ML) are the total energies of bulk structures and monolayer, respectively. The results are summarized in **Table S9** with corresponding lattice parameters.

For **Cyclo-**structures, the most stable AA and AB stacking structures have close E_{int} thus their band structures are calculated. For **Glaser**-structures, AA stacking structures are always more stable than AB structures thus only the band structures of AA structures are calculated. The band gaps are also summarized in **Table S9**. The corresponding views of **Cyclo**- and **Glaser**-structures are shown in **Figure S24** and **S25**, respectively. The band structures calculated for **Cyclo** and **Glaser**-compositions are shown in **Figure S26** and **S27**, respectively.

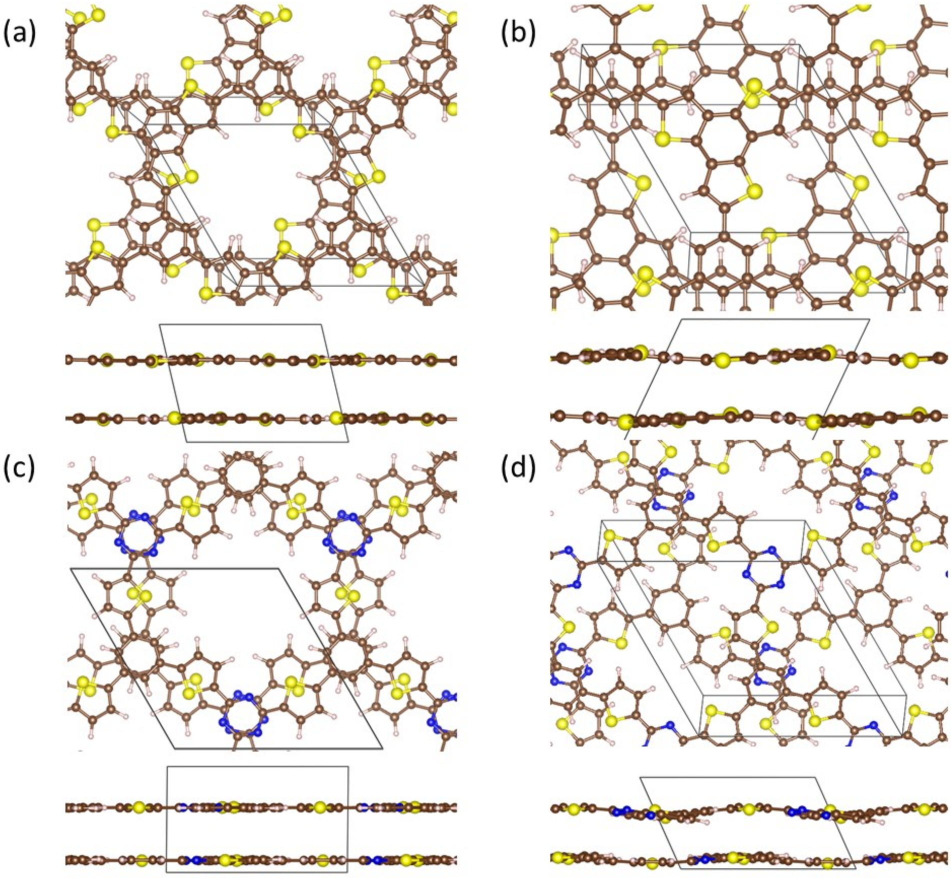

Figure S16. The top and side views of bulk structures of (a) **BTT-Cyclo** AA-2; (b) **BTT-Cyclo** AB-2; (c) **Tz-Th-Cyclo** AA-2 and (d) **Tz-Th-Cyclo** AB-2. Blue, brown, yellow and white indicate N, C, S and H atoms, respectively.

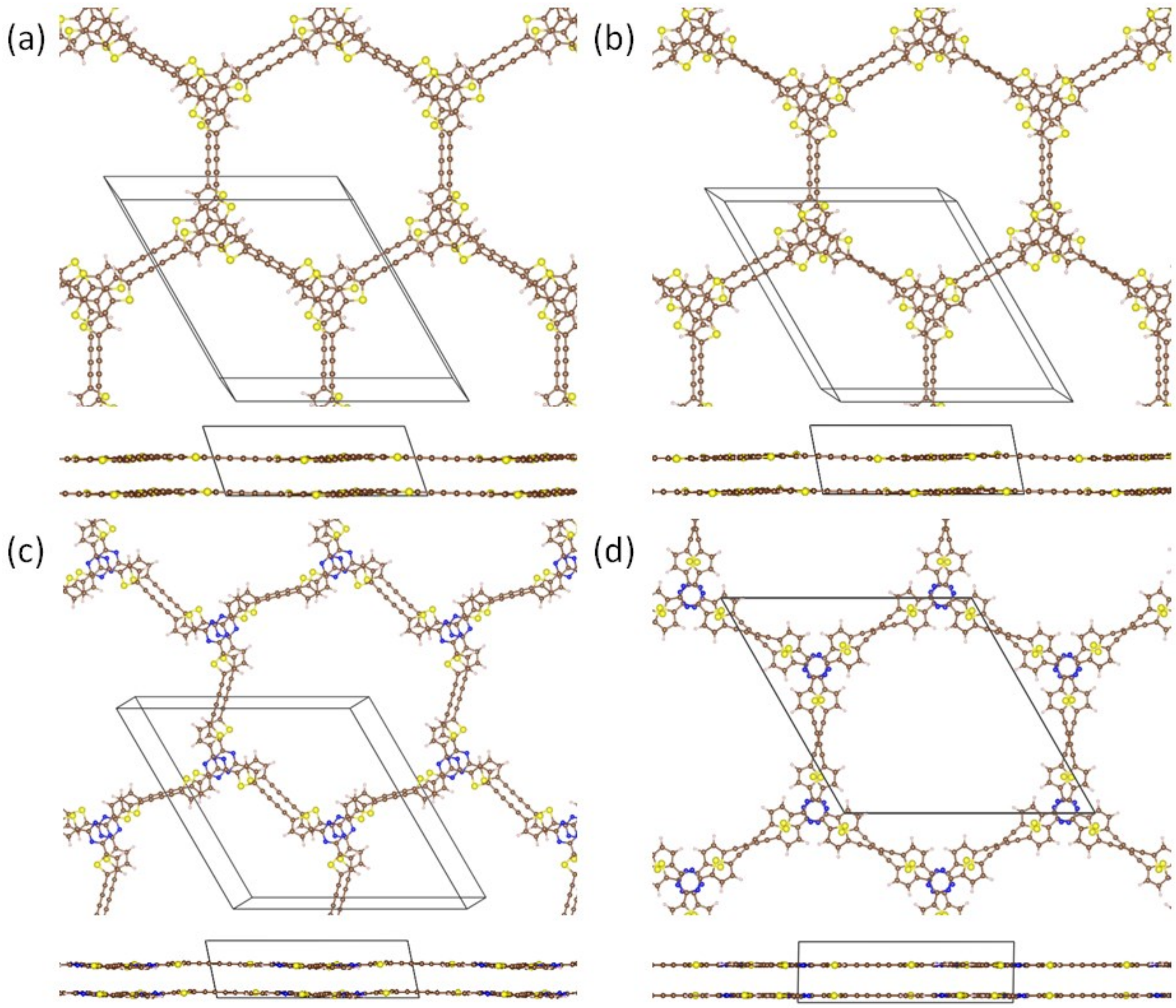

Figure S17. The top and side views of bulk structures of (a) **BTT-Glaser** AA-1; (b) **BTT-Glaser** AA-2; (c) **Tz-Th-Glaser** AA-1 and (d) **Tz-Th-Glaser** AA-2. Blue, brown, yellow and white indicate N, C, S and H atoms, respectively.

Table S5. The interaction energies (E_{int}), lattice parameters and band gaps (ΔE_{gap}) of monolayers and bulk structures

	E_{int}/kJ mol^{-1}	Lattice parameter						E_{gap}/eV
		a/Å	*b*/Å	*c*/Å	*α*/°	*β*/°	*γ*/°	
BTT-Cyclo								
monolayer	–	11.11	11.11	–	90	90	120	2.15
AA-1	−184	11.09	11.09	7.59	96	107	120	–
AA-2	−185	11.09	11.09	7.41	109	75	120	1.91
AB-1	−172	11.09	11.09	6.91	90	90	120	–
AB-2	−186	11.09	11.07	7.15	69	89	120	1.95
BTT-Glaser								
monolayer-1	–	23.62	23.67	–	90	90	120	1.88
monolayer-2	–	23.63	23.67	–	90	90	120	1.88
AA-1	−297	23.66	23.60	7.55	112	77	120	1.30
AA-2	−304	23.65	23.65	7.36	107	74	120	1.36
AB-1	−171	23.83	23.67	7.01	97	103	121	–
AB-2	−152	23.64	23.64	7.05	90	90	120	–
Tz-Th-Cyclo								
monolayer	–	13.73	13.73	–	90	90	120	2.23
AA-1	−165	13.71	13.71	7.43	90	90	120	–
AA-2	−218	13.70	13.70	6.93	90	90	120	1.62
AB-1	−197	13.70	13.69	6.66	90	90	120	–
AB-2	−208	13.69	13.64	6.76	109	93	120	1.93
Tz-Th-Glaser								
monolayer-1	–	28.96	28.50	–	90	90	120	1.60
monolayer-2	–	28.81	28.92	–	90	90	120	1.59
AA-1	−356	28.84	28.66	7.51	90	108	120	1.19
AA-2	−353	28.88	28.60	7.03	89	90	120	1.04
AB-1	−187	28.89	28.51	6.46	90	91	120	–
AB-2	−187	28.91	28.56	6.56	91	90	120	–

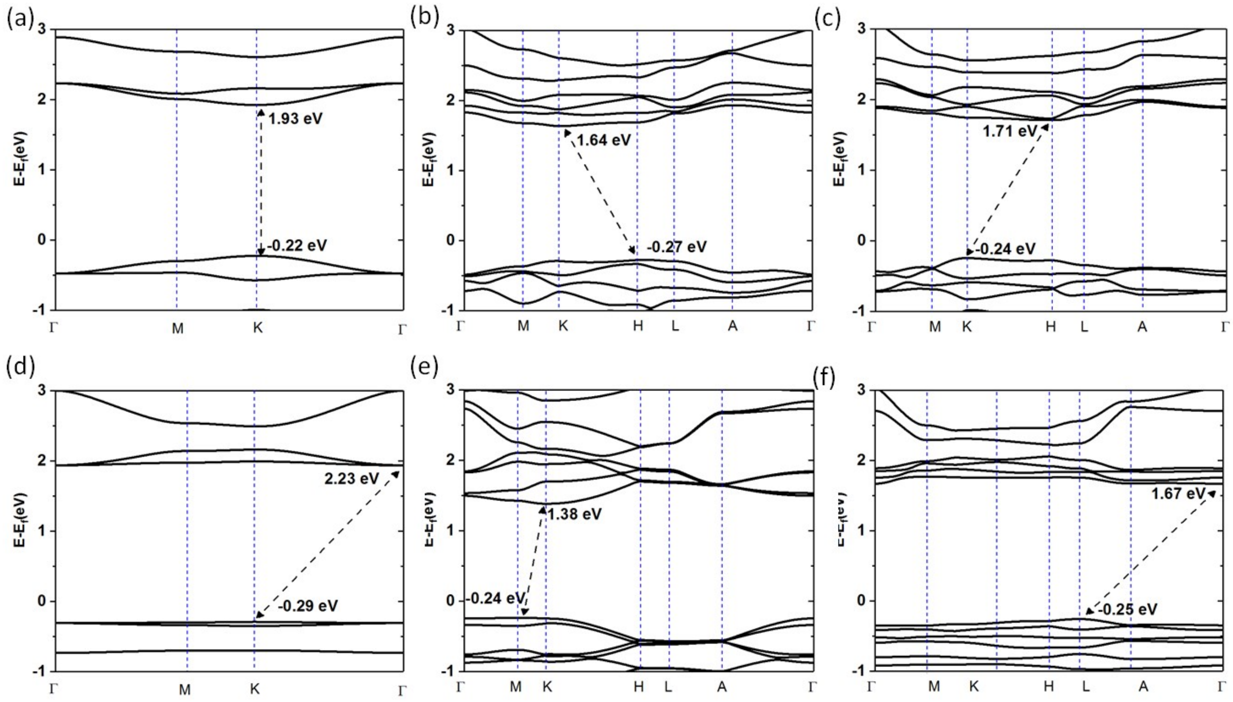

Figure S18. Calculated band structures for **Cyclo**-structures: (a) **BTT-Cyclo** monolayer; (b) **BTT-Cyclo** AA-2; (c) **BTT-Cyclo** AB-2; (d) **Tz-Th-Cyclo** monolayer; (e) **Tz-Th-Cyclo** AA-2 and (f) **Tz-Th-Cyclo** AB-2.

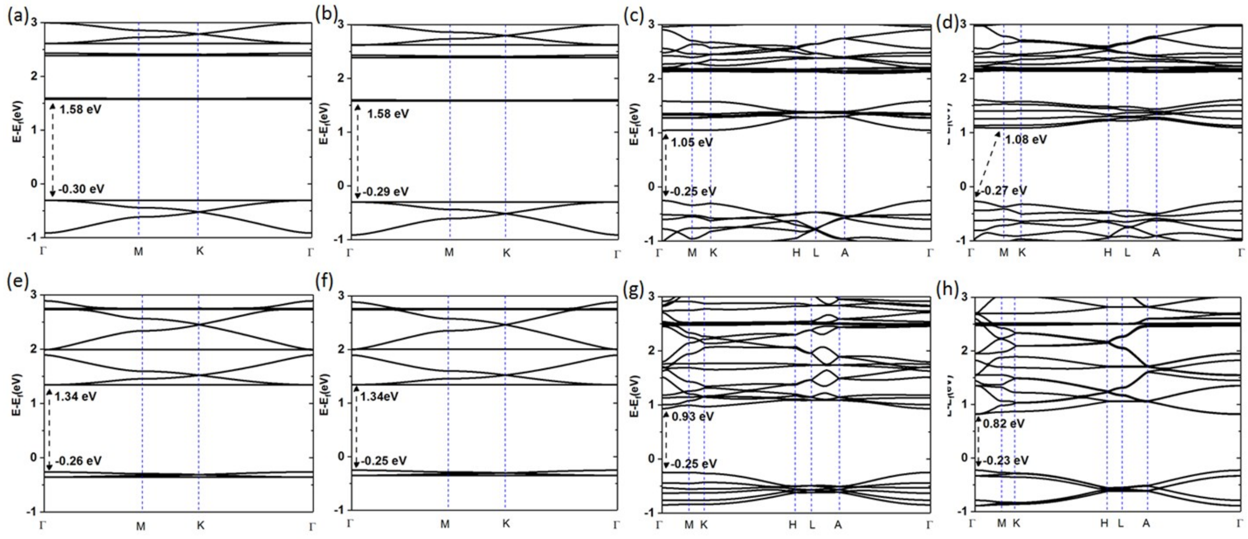

Figure S19. Calculated band structures for **Glaser**-structures: (a) **BTT**-**Glaser** monolayer-1; (b) **BTT**-**Glaser** monolayer-2; (c) **BTT**-**Glaser** AA-1; (d) **BTT**-**Glaser** AA-2; (e) **Tz-Th-Glaser** monolayer-1; (f) **Tz-Th**-**Glaser** monolayer-2; (g) **Tz-Th**-**Glaser** AA-1 and (h) **Tz-Th**-**Glaser** AA-2.

Band edges simulation

Band edges were calculated and aligned *vs.* vacuum considering the dependence of water splitting redox potentials on the pH level:

$E_{O2/H2O}^{ox}= -5.67$ eV$+0.059\times$pH,
$E_{H+/H2}^{red}= -4.44$ eV$+0.059\times$pH.
Energy levels of conduction band minimum (CBM) and valence band maximum (VBM) were obtained according to following equations:

$E'_{CBM}=-\varphi+E_{CBM,}$
$E'_{VBM}=-\varphi+E_{VBM,}$
where $E_{CBM/VBM}$ is CBM and VBM directly obtained from the band structure calculations, φ is the work function calculated for each polymer monolayer.

Photoelectrochemical Performance

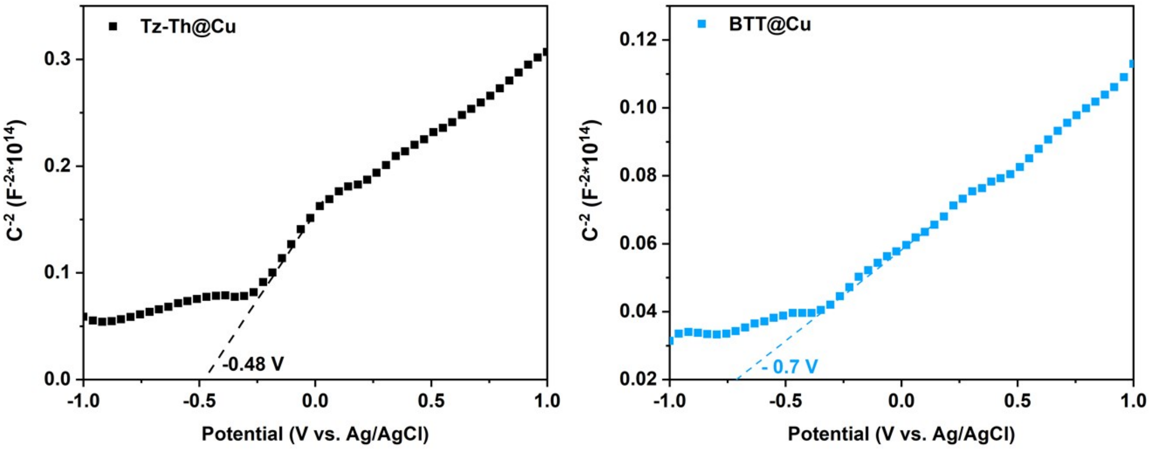

Figure S20. Mott-Schottky plots recorded at 1.5 kHz frequency for Tz-Th@Cu |(black) and BTT@Cu (blue) (measured in 0.01 M Na2SO4, pH = 7 vs. Ag/AgCl reference electrode).

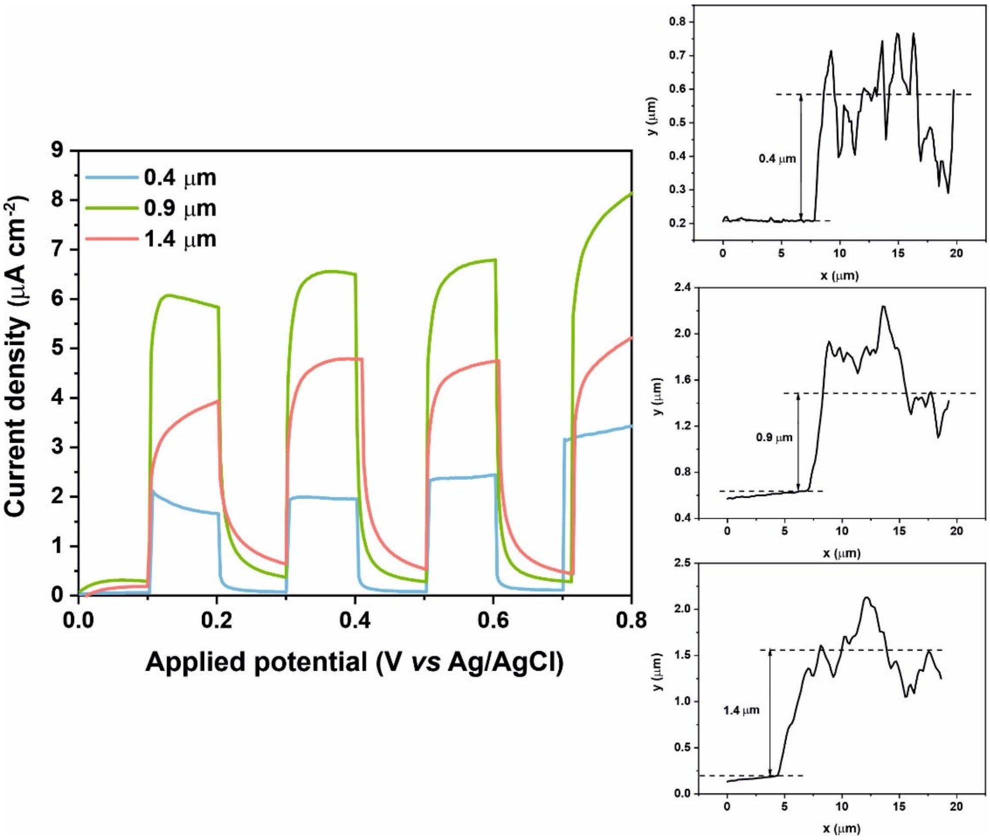

Figure S21. Electrode thickness study for **Tz-Th@Cu.** On the left – photocurrent density measurements, on the right – surface profiles of polymer coatings obtained *via* AFM.

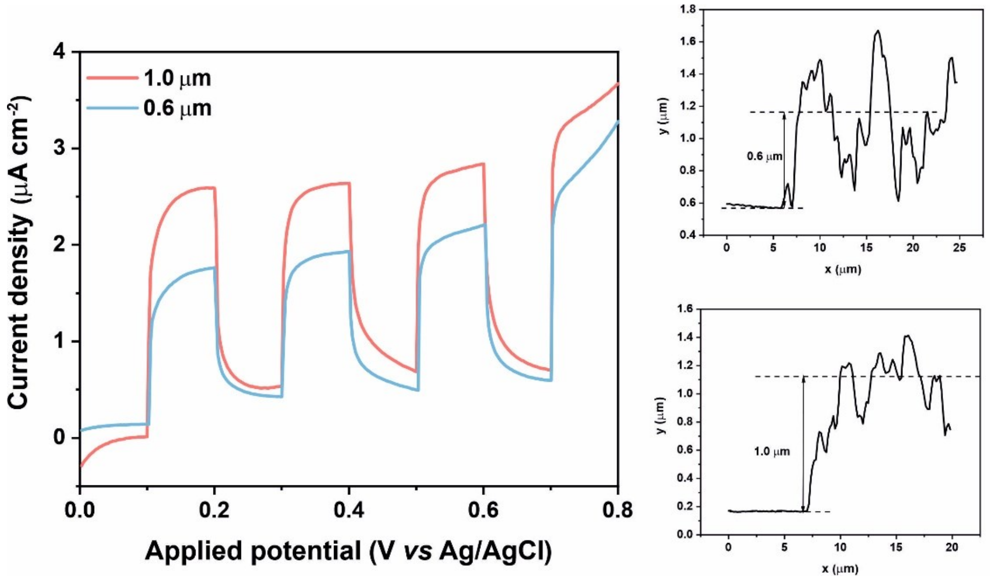

Figure S22. Electrode thickness study for **BTT@Cu.** On the left – photocurrent density measurements, on the right – surface profiles of polymer coatings obtained *via* AFM. and the attempts to prepare thicker coating resulted in unstable polymer films, which were easily detached from the ITO substrate when exposed to the electrolyte solution. Possibly, thicker films of **BTT@Cu** become too heavy to be properly attached to the ITO and fall of from the electrode due to the relatively apolar, hence, poorly wettable polymer structure.

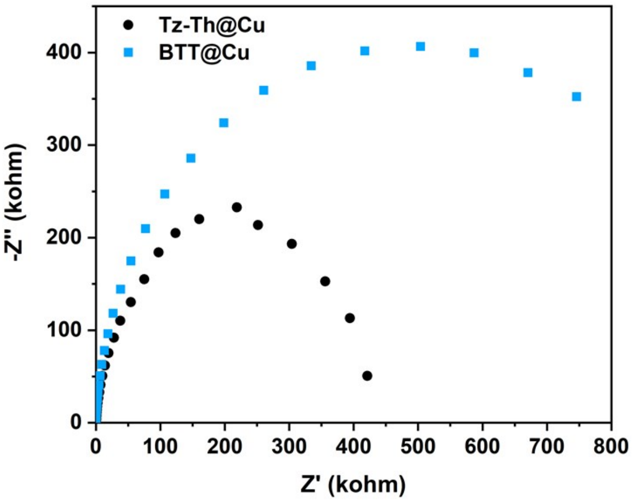

Figure S23. EIS Nyquist plots at applied voltage of 0.6 V under illuminated conditions recorded for **Tz-Th@Cu** (blue) and **BTT@Cu** (black).

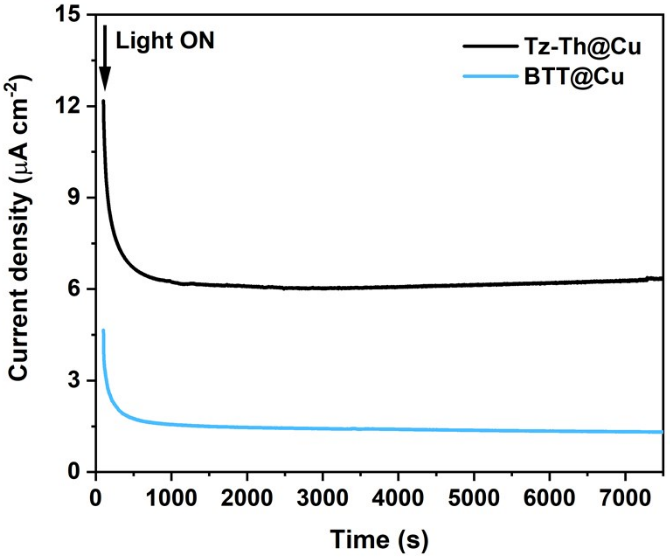

Figure S24. Stability test showing photocurrent current density retaining efficiency of **Tz-Th@Cu** (black) and **BTT@Cu** (blue) for 7500 seconds (measured at 0.6 V vs. Ag/AgCl reference electrode in 0.01 M Na_2SO_4, pH = 6.8).

Table S6. Comparison of experimental setups and achieved photocurrent density of several benchmark organic metal-free photoelectrodes with the results of the current work.

Material	Photocurrent density (μA cm^{-2})	Applied potential (V vs. Ag/AgCl)	Light source	Donor-acceptor composition	Ref.
g-C_3N_4	0.3	-1.0	300 W Xenon lamp λ > 420 nm	No	11
g-C_3N_4	1.2	-0.2	150 W Xe lamp λ > 420 nm	No	12
g-C_3N_4@C	0.7	-0.1	Keithley 6300 semiconductor analyzer	No	13
C,O-g-C_3N_4	0.4	-0	300 W xenon arc lamp, 100 mW cm^{-2}	No	14
Red phosphorus	0.09	-1.0	Cole-Parmer illuminator, 41720 series, 200 mW cm^{-2}	No	15
Microfibrous phosphorus	0.35	-0.4	300 W Xenon lamp 100 mW cm^{-2}	No	16
$B_{4.3}C$	46	-0.76	300 W Xenon lamp 64 mW cm^{-2}	No	17
$B_{13}C_2$	16	-0.76	300 W Xenon lamp 64 mW cm^{-2}	No	17
PTEB	10	-0.3	200 W Xenon lamp 100 mW cm^{-2}	No	18
Tz-Th@Cu	**6.8**	**0.6**	**300 W Xenon lamp** **100 mW cm^{-2}**	**Yes**	**This work**
BTT@Cu	**2.3**	**0.6**	**300 W Xenon lamp** **100 mW cm^{-2}**	No	**This work**
Tz-Th$_b$	**3.7**	**0.6**	**300 W Xenon lamp** **100 mW cm^{-2}**	**Yes**	**This work**
BTT$_b$	**2.6**	**0.6**	**300 W Xenon lamp** **100 mW cm^{-2}**	No	**This work**

Applied potentials were recalculated *vs*. to Ag/AgCl electrode (if stated *vs*. RHE) *via* following equation: $E_{RHE} = E_{Ag/AgCl} + 0.059\ pH + E_{Ag/AgCl}^0$ ($E_{Ag/AgCl}^0 = 0.199$ V).

Contact angle measurements

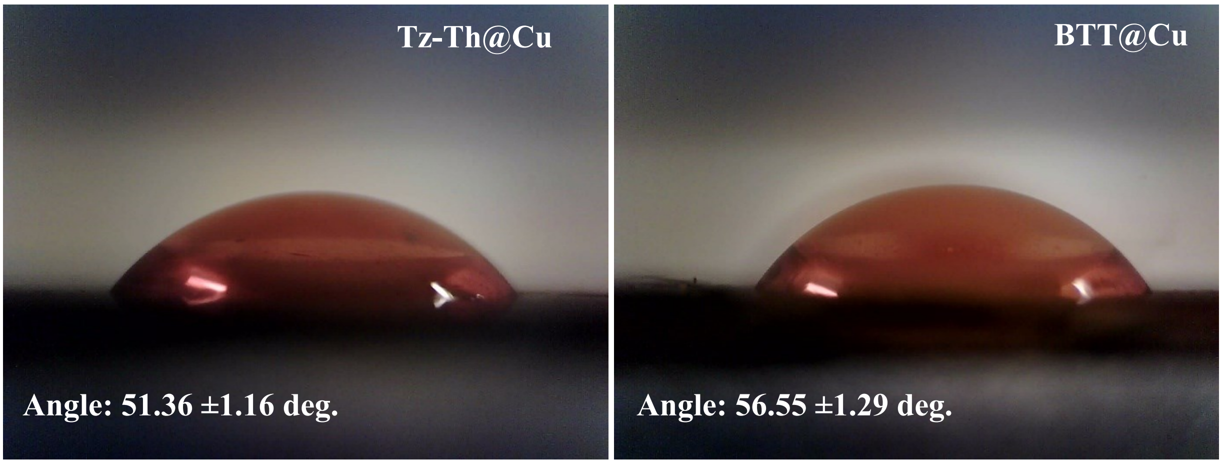

Figure S25. Average contact angle of a sessile water drops on **Tz-Th@Cu** (left) and **BTT@Cu** (right), grown on copper deposited onto silicon wafer.

Photoelectrochemical O_2 evolution

Gas chromatography (GC) measurements were performed in a gas-tight H-cell with 1 M NaOH electrolyte and Ag/AgCl reference electrode. The working electrodes were prepared by spray coating of active material on ITO substrate. Bare ITO surface was covered with a Teflon tape to avoid the influence of ITO on the produced photocurrent. Chronoamperometry was applied at potential 0.9 V to maintain constant production of oxygen. Meanwhile, Ar was constantly purged into the compartment containing the working electrode connected to the gas-sampling loop of a valve-gas chromatograph (Agilent 7890B). A thermal conductivity detector (TCD) was used to detect the generated oxygen, which we attributed to signals with retention times between 1.37 and 1.42 min (Figure S22).[19-23]

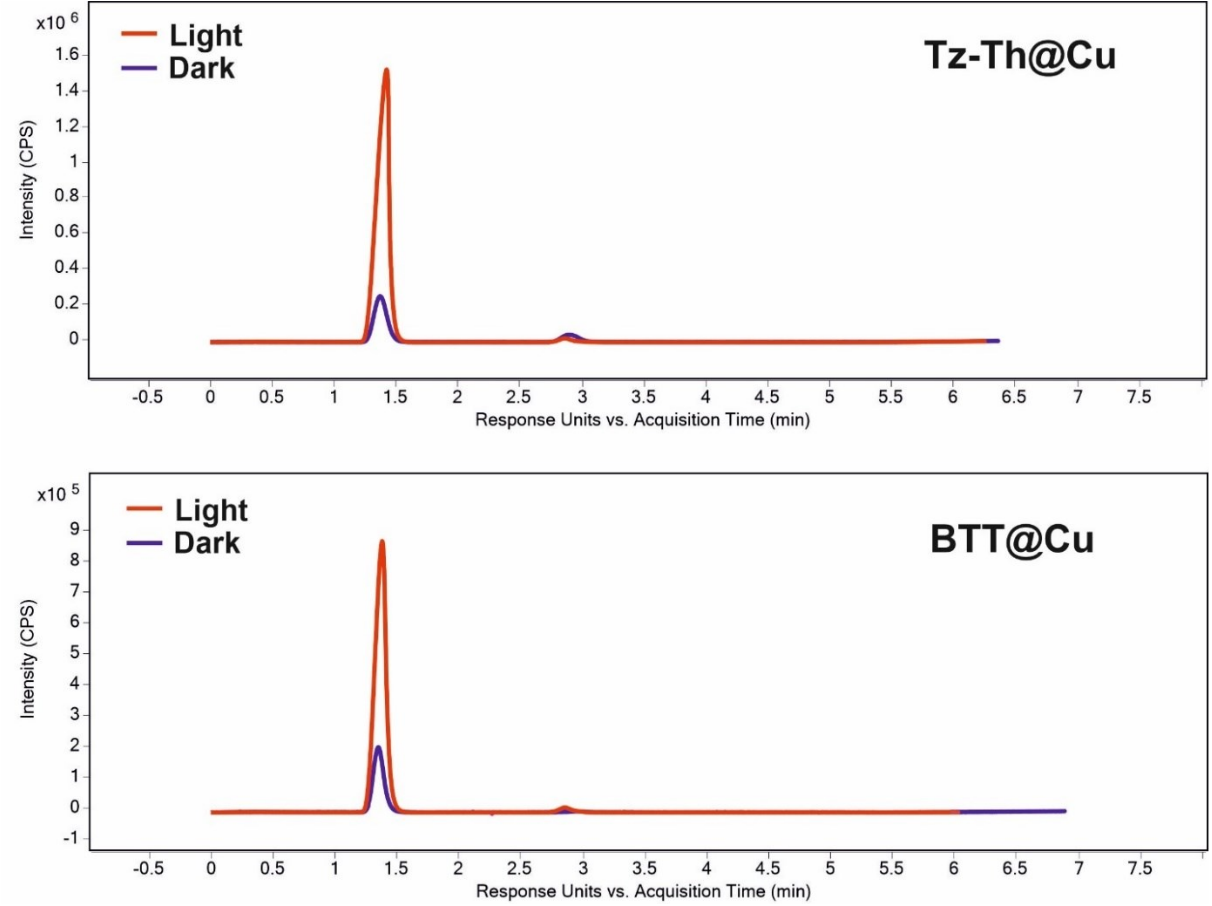

Figure S26. GC spectra recorded for **Tz-Th@Cu** (up) and **BTT@Cu** (bottom) under dark (blue lines) and illuminated (red lines) conditions.

Table S7. Comparison of oxygen evolution ion efficiency for prepared materials derived from the corresponding area under O_2 peaks in GC spectra

Material	Peak area (Dark)(a.u.)	Peak area (Light) (a.u.)	Ratio Light/Dark
Tz-Th@Cu	1939318.8 (rt* 1.37)	11050480.62 (rt* 1.42)	5.7
BTT@Cu	1313299.3 (rt*1.35)	5666303.35 (rt* 1.38)	4.3

*rt – retention time in minutes

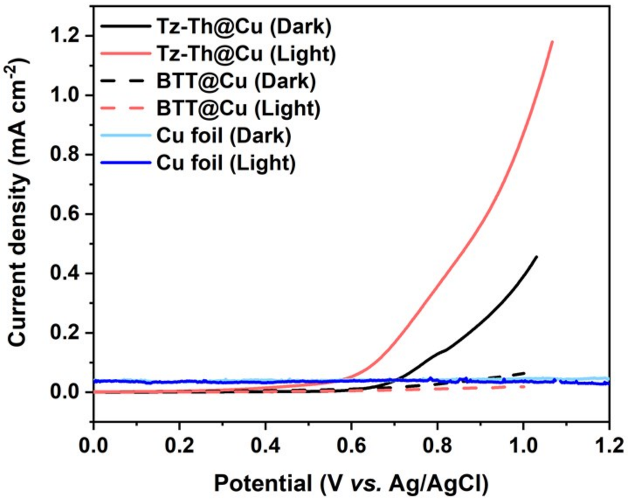

Figure S27. Comparison of the performance of **Tz-Th@Cu** and **BTT@Cu** in the OER with conventional copper foil, which was used for polymer synthesis. The use of Cu foil as a working electrode resulted in a low current of ~0.03 mA cm^{-2}, which is comparable to **BTT@Cu** (at 1 V *vs* Ag/AgCl), however, is significantly lower the that of **Tz-Th@Cu**. Moreover, we observed no increase in the current at any potential, which shows that copper has no catalytic activity in the electrochemical OER process.

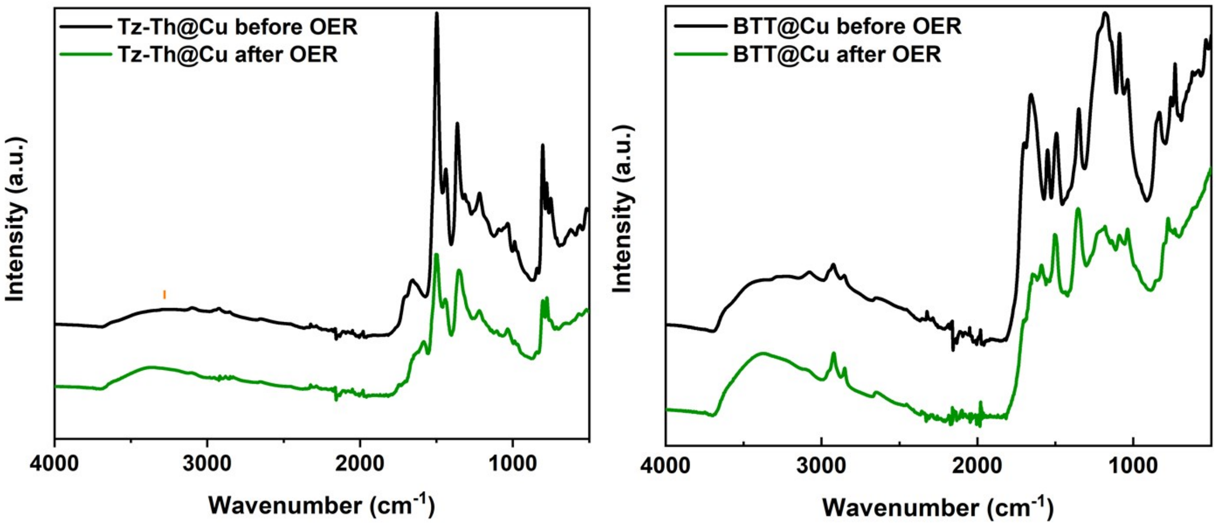

Figure S28. FTIR spectra recorded for **Tz-Th@Cu** (left) and **BTT@Cu** (right) before and after OER experiment (under illuminated conditions). No additional peaks appeared in the region from 2000 to 3000 cm^{-1}, as well as main characteristic peaks remained in the fingerprint region (600-1500 cm^{-1}), confirming the structural stability of both polymers under OER conditions.

Bulk Materials Characterisation

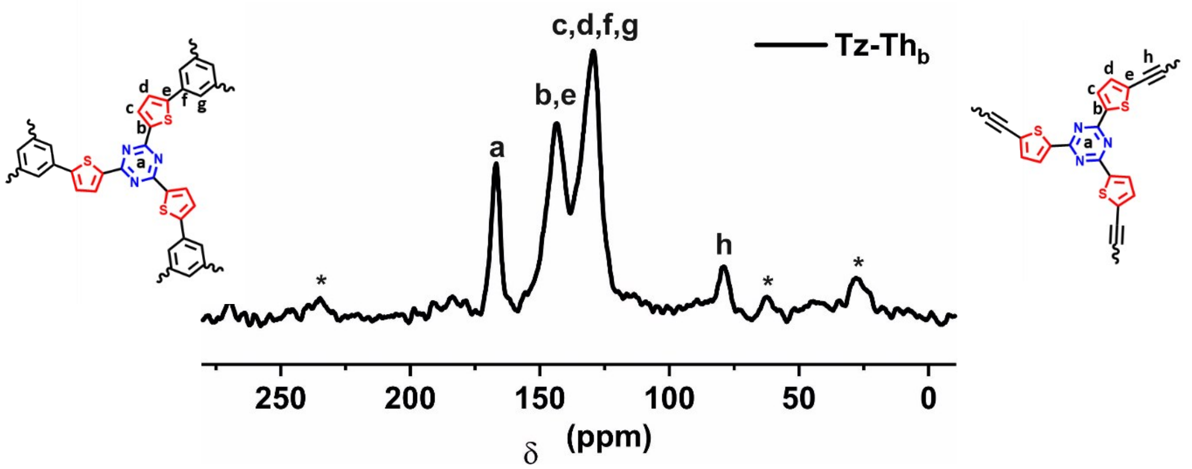

Figure S29. Solid-state ^{13}C CP-MAS spectra of **Tz-Th$_b$.** Spinning sidebands are marled with an asterisk (*).

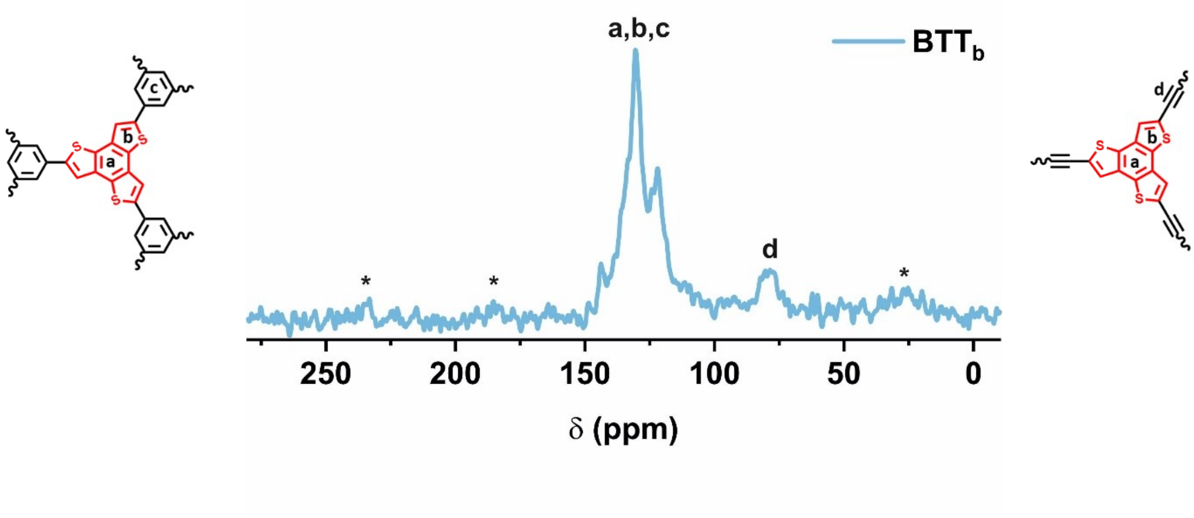

Figure S30. Solid-state ^{13}C CP-MAS spectra of **BTT$_b$**. Spinning sidebands are marled with an asterisk (*).

Table S8. EA and ICP-OES data (in wt%) for **Tz-Th$_b$**

Elemental composition	**C**	**H**	**N**	**S**	**C/N**	**C/S**	**Cu**	**P**
Theoretical	**63.62**	**1.53**	**10.60**	**24.26**	**6.00**	**2.62**	0.3	0.35
Found	57.96	2.58	10.04	18.02	5.77	3.21		

Table S9. EA and ICP-OES data (in wt%) for **BTT$_b$**

Elemental composition	**C**	**H**	**N**	**S**	**C/S**	**Cu**	**P**
Calculated	**68.55**	**0.96**	**-**	**30.49**	**2.25**	3.06	n/d*
Found	53.39	2.33	1.61	19.96	2.67		

*n/d – not detected

Table S10. EDS data (in wt%) for **Tz-Th$_b$**

Elemental composition	**C**	**H**	**N**	**S**	**C/N**	**C/S**	**Cu**	O
Calculated	**63.62**	**1.53**	**10.60**	**24.26**	**6.00**	**2.62**	1.0	13.9
Found	45.20	n/a*	27.60	11.50	1.63	3.93		

Table S11. EDS data (in wt%) for **BTT$_b$**

Elemental composition	**C**	**H**	**N**	**S**	**C/S**	**Cu**	O
Calculated	**68.55**	**0.96**	**-**	**30.49**	**2.25**	2.34	9.23
Found	74.92	n/a*	n/d	13.34	5.61		

*n/a – not analysed

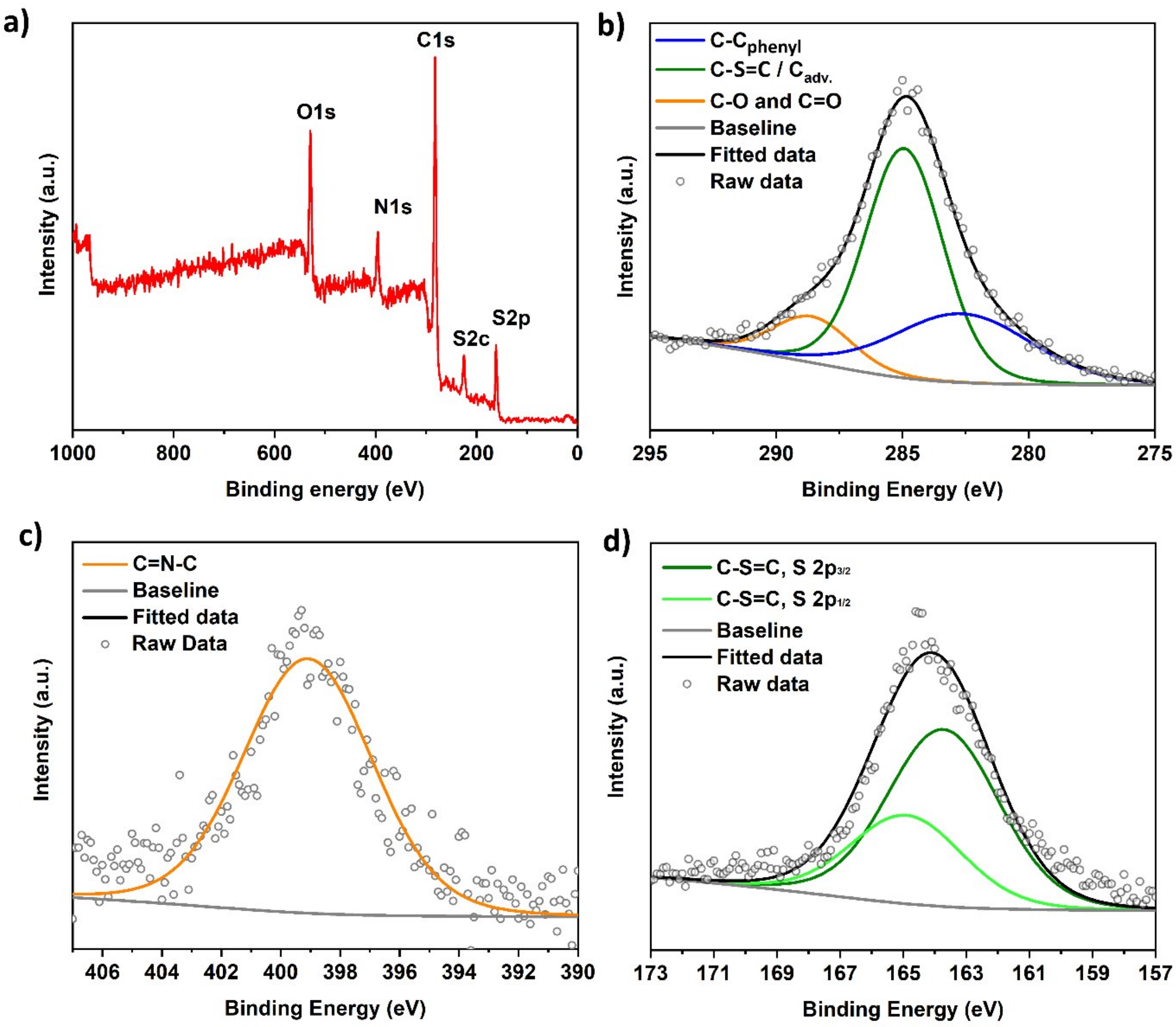

Figure S31. XPS spectra of **Tz-Th$_b$**: (**a**) survey spectra; high resolution deconvoluted spectra of C 1s (**b**), N 1s (**c**), and S 2p (**d**) regions.

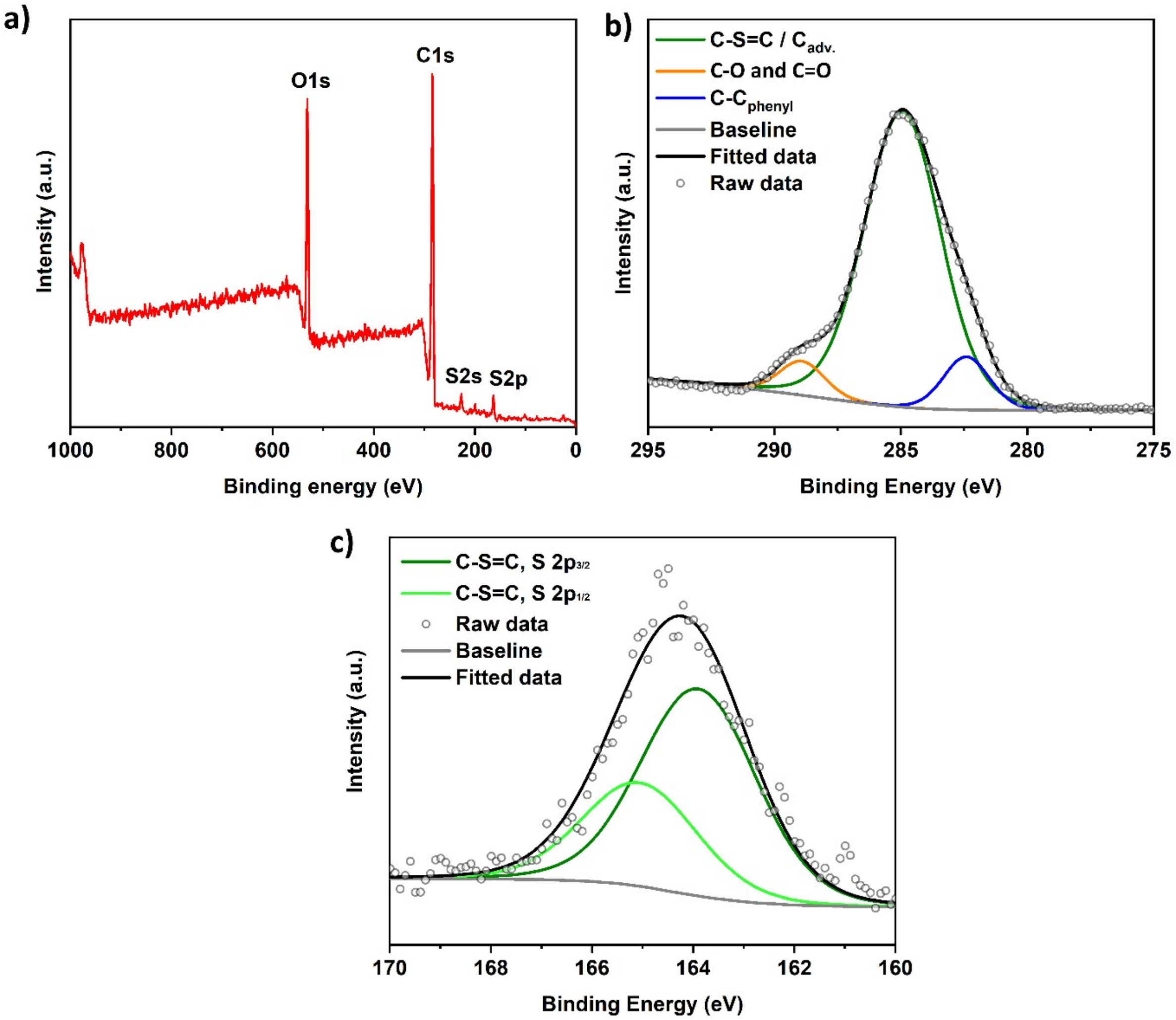

Figure S32. XPS spectra of **BTT$_b$**: (**a**) survey spectra; high resolution deconvoluted spectra of C 1s (**b**) and S 2p (**c**) regions.

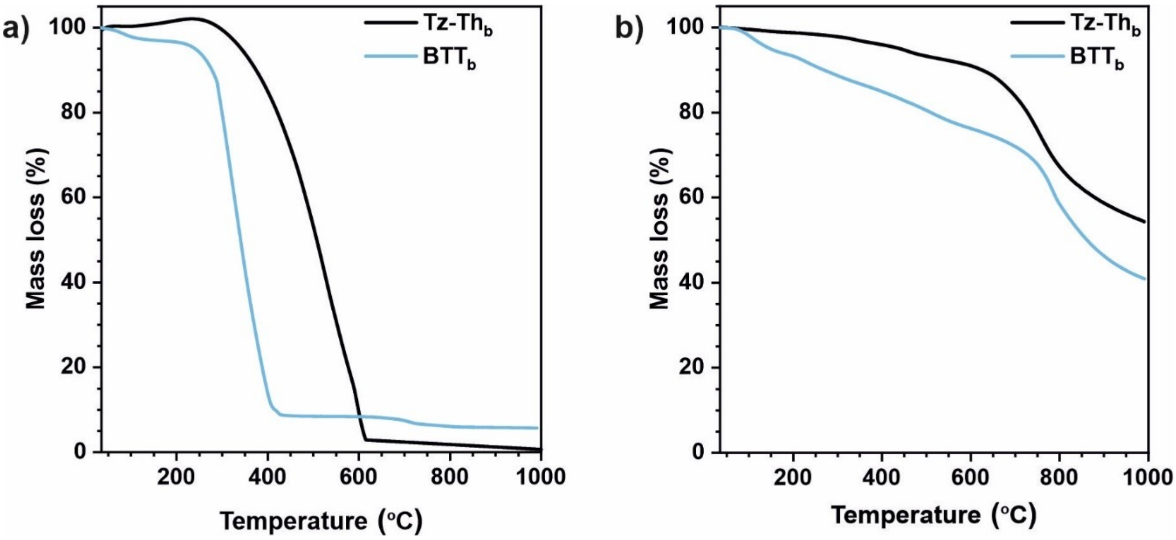

Figure S33. TGA data of **Tz-Th$_b$** (black) and **BTT$_b$** (blue) polymers heated up to 1000 °C with heating rate of 10 deg. min^{-1} under air **(a)** and heated under N_2 **(b)** atmosphere.

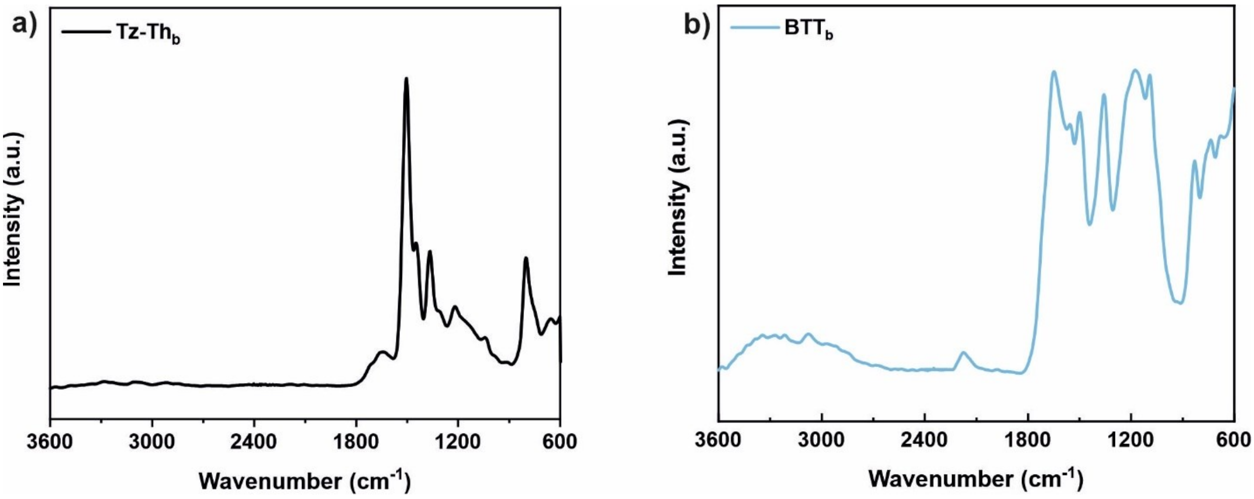

Figure S34. FTIR spectra of prepared materials and respective molecular precursors.

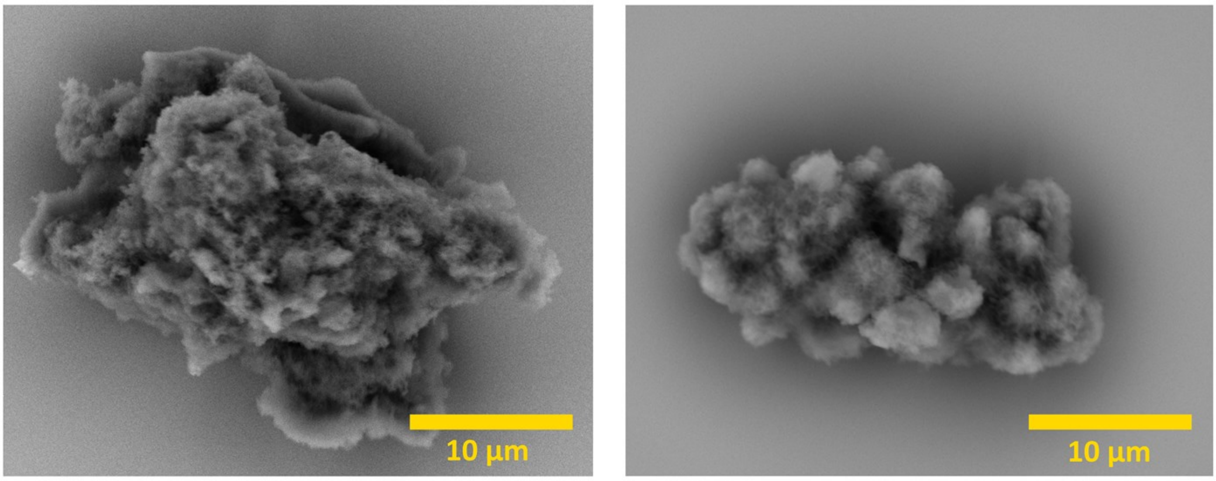

Figure S35. SEM images of bulk particles of **Tz-Th$_b$** (left) and **BTT$_b$** (right) polymers.

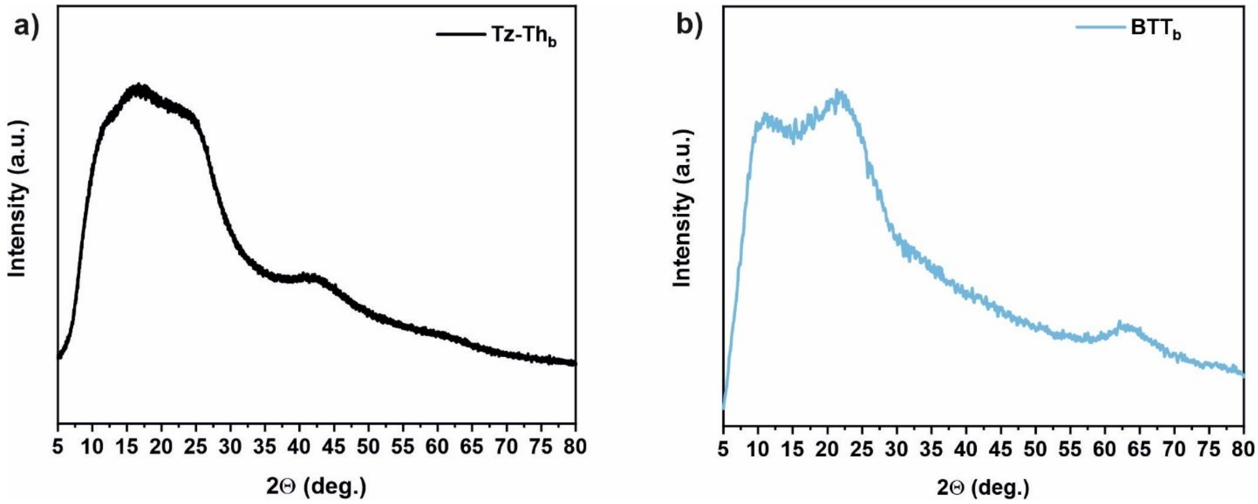

Figure S36. PXRD patterns of **Tz-Th@Cu** (a) and **BTT@Cu** (b) in the range from 0 to 80 deg. 2θ.

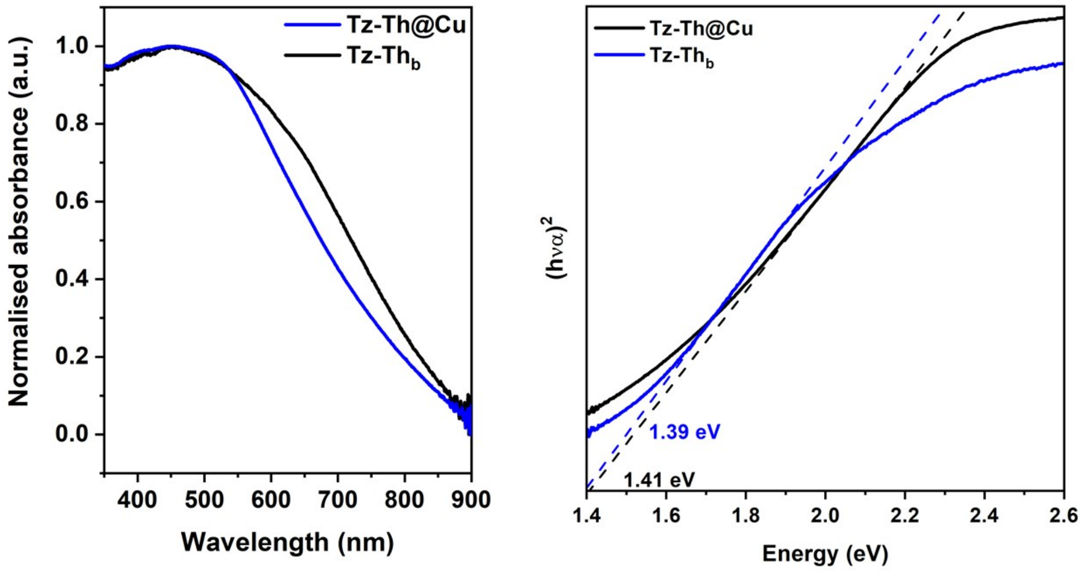

Figure S37. Diffuse reflectance solid-state UV-Vis spectra (left) and Tauc plots (right) of **Tz-Th@Cu** and **Tz-Th_b** polymers.

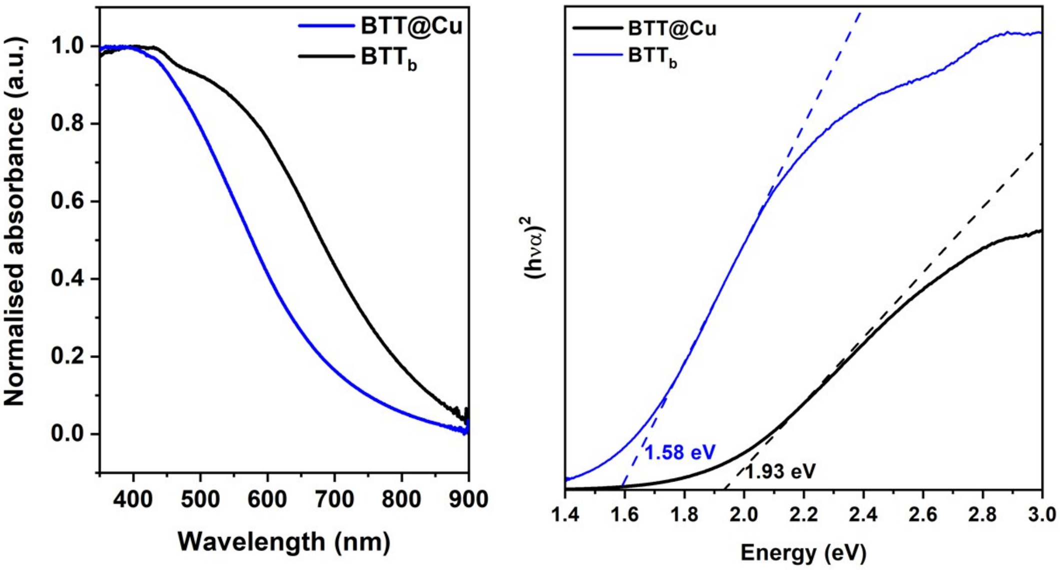

Figure S38. Diffuse reflectance solid-state UV-Vis spectra (left) and Tauc plots (right) of **Tz-Th@Cu** and **Tz-Th$_b$** polymers.

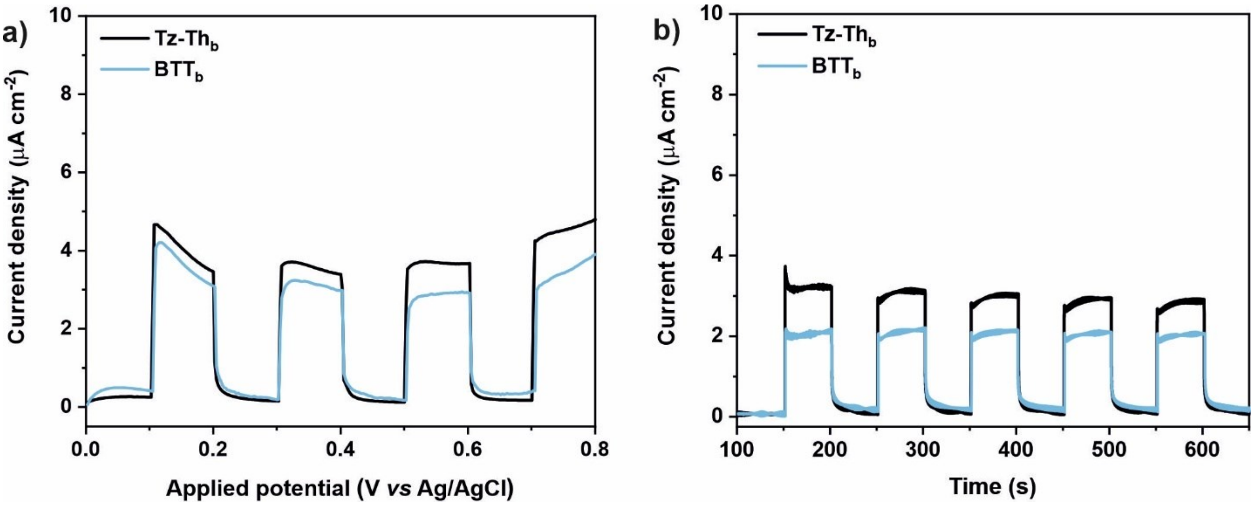

Figure S39. a) Current density-potential curves vs. applied potential of **Tz-Th$_b$** (black) and **BTT$_b$** (blue). under intermittent irradiation; b) Transient current density *vs*. time at 0.6 V applied potential under intermittent light irradiation recorded for both materials ((a) and (b) measured in 0.01 M Na_2SO_4, pH = 6.8 vs. Ag/AgCl reference electrode).

References

1. T. Yasuda, T. Shimizu, F. Liu, G. Ungar and T. Kato, *JACS*, 2011, **133**, 13437-13444.
2. R. Maragani and R. Misra, *Tetrahedron Lett.*, 2013, **54**, 5399-5402.
3. Y. S. Kochergin, D. Schwarz, A. Acharjya, A. Ichangi, R. Kulkarni, P. Eliášová, J. Vacek, J. Schmidt, A. Thomas and M. J. Bojdys, *Angew. Chem. Int. Ed.*, 2018, **57**, 14188–14192.
4. T. Kashiki, M. Kohara, I. Osaka, E. Miyazaki and K. Takimiya, *J. Org. Chem.*, 2011, **76**, 4061-4070.
5. E. Y.-H. Hong, H.-L. Wong and V. W.-W. Yam, *Chem. - Eur. J.*, 2015, **21**, 5732-5735.
6. J. P. Perdew, K. Burke and M. Ernzerhof, *Physical Review Letters*, 1996, **77**, 3865-3868.
7. P. E. Blöchl, *Physical Review B*, 1994, **50**, 17953-17979.
8. G. Kresse and J. Furthmüller, *Computational Materials Science*, 1996, **6**, 15-50.
9. G. Kresse and D. Joubert, *Physical Review B*, 1999, **59**, 1758-1775.
10. H. J. Monkhorst and J. D. Pack, *Physical Review B*, 1976, **13**, 5188-5192.
11. Y. F. Guo, J. Li, Y. P. Yuan, L. Li, M. Y. Zhang, C. Y. Zhou and Z. Q. Lin, *Angew Chem Int Edit*, 2016, **55**, 14693-14697.
12. Y. J. Zhang, A. Thomas, M. Antonietti and X. C. Wang, *J Am Chem Soc*, 2009, **131**, 50-+.
13. Q. Han, B. Wang, J. Gao and L. T. Qu, *Angew Chem Int Edit*, 2016, **55**, 10849-10853.
14. D. K. L. Chana and J. C. Yu, *Catalysis Today*, 2017, DOI: https://doi.org/10.1016/j.cattod.2017.05.017.
15. F. Wang, W. K. H. Ng, J. C. Yu, H. J. Zhu, C. H. Li, L. Zhang, Z. F. Liu and Q. Li, *Appl Catal B-Environ*, 2012, **111**, 409-414.
16. Z. Hu, L. Yuan, Z. Liu, Z. Shen and J. C. Yu, *Angew. Chem. Int. Ed.*, 2016, **55**, 9580-9585.
17. J. K. Liu, S. H. Wen, Y. Hou, F. Zuo, G. J. O. Beran and P. Y. Feng, *Angew Chem Int Edit*, 2013, **52**, 3241-3245.
18. T. Zhang, Y. Hou, V. Dzhagan, Z. Liao, G. Chai, M. Löffler, D. Olianas, A. Milani, S. Xu, M. Tommasini, D. R. T. Zahn, Z. Zheng, E. Zschech, R. Jordan and X. Feng, *Nat Commun*, 2018, **9**, 1140.
19. R. Firor, *Hewlett-Packard Company, Application Note*, 1990, 228-124.
20. Z. Ji and I. Chang, *Hewlett-Packard Company, Application Note*, 1994, 228-286.
21. Y. Zhou and C. Wang, *Agilent Technologies, Application Note* 2003, 5988-9259.
22. X. Li, *Agilent Technologies (Shanghai) Co., Ltd, Application Note HPI*, 2008.
23. Z. Ji, *Agilent Technologies, Application Note* 2012, 228-387.